North Atlantic temperature change across the Eocene-Oligocene Transition

Ilja Japhir Kocken[1], Peter Dirk Nooteboom[2], Kasper van der Veen[1], Inigo A Müller[3], Anna Nele Meckler[4], and Martin Ziegler[1]

[1]Utrecht University
[2]Institute of Marine and Atmospheric Research Utrecht
[3]Université de Genève
[4]University of Bergen

November 22, 2022

Abstract

The Eocene–Oligocene transition (˜34 Ma), is marked by the rapid development of a semi-permanent Antarctic ice-sheet, as indicated by ice-rafted debris. Proxy reconstructions indicate a drop in atmospheric CO2 and global cooling. How these changes affected sea surface temperatures in the North Atlantic and ocean water stratification remains poorly constrained. In this study, we apply clumped-isotope thermometry to well-preserved planktic foraminifera, that are associated with mixed-layer and thermocline dwelling depths from the drift sediments at IODP Site 1411, Newfoundland, across four intervals bracketing the EOT. The mixed-layer dwelling foraminifera record a cooling of 2.2 ± 2.4 °C (mean ± 95% CI) across the EOT. While the cooling amplitude is similar to previous SST reconstructions, absolute temperatures (Eocene 20.0 ± 2.7 °C, Oligocene 18.0 ± 2.1 °C) appear colder than what is expected for this location based on previously reconstructed SSTs for the northernmost Atlantic. We discuss seasonal bias, recording depth, and appropriate consideration of paleolatitudes, all of which complicate the comparison between SST reconstructions and model output. Thermocline dwelling foraminifera record a larger cooling across the EOT (Eocene 19.0 ± 3.4 °C, Oligocene 14.0 ± 3.1 °C, cooling of 5.2 ± 3.2 °C), than foraminifera from the mixed layer, consistent with an increase in ocean stratification which may be related to the onset or intensification of the Atlantic meridional overturning circulation.

North Atlantic temperature change across the Eocene–Oligocene Transition

Ilja J. Kocken[1], Peter D. Nooteboom[2], Kasper van der Veen[1], Inigo A. Müller[1], A. Nele Meckler[3], Martin Ziegler[1]

[1]Department of Earth Sciences, Faculty of Geosciences, Utrecht University, Princetonlaan 8a, 3584 CB, Utrecht, the Netherlands.

[2]Department of Physics, Faculty of Science, Utrecht University, Institute for Marine and Atmospheric Research Utrecht (IMAU), the Netherlands

[3]Department of Earth Science, Bjerknes Centre for Climate Research, University of Bergen, Realfagbygget, Allégt. 41, 5020 Bergen, Norway

Key Points:

- Clumped isotopes from well-preserved planktic foraminifera show 2.2 K cooling across the EOT of the mixed layer in the North Atlantic.
- Mixed layer temperatures for the Eocene (20 °C) and the Oligocene (18 °C) are cooler than previous estimates.
- Intensified thermocline cooling compared to the mixed layer indicates increased stratification after the EOT, hinting at intensified AMOC.

Corresponding author: Ilja J. Kocken, `i.j.kocken@uu.nl`

Abstract

The Eocene–Oligocene transition (∼34 Ma), is marked by the rapid development of a semi-permanent Antarctic ice-sheet, as indicated by ice-rafted debris. Proxy reconstructions indicate a drop in atmospheric CO_2 and global cooling. How these changes affected sea surface temperatures in the North Atlantic and ocean water stratification remains poorly constrained. In this study, we apply clumped-isotope thermometry to well-preserved planktic foraminifera, that are associated with mixed-layer and thermocline dwelling depths from the drift sediments at IODP Site 1411, Newfoundland, across four intervals bracketing the EOT. The mixed-layer dwelling foraminifera record a cooling of 2.2 ± 2.4 °C (mean ± 95% CI) across the EOT. While the cooling amplitude is similar to previous SST reconstructions, absolute temperatures (Eocene 20.0 ± 2.7 °C, Oligocene 18.0 ± 2.1 °C) appear colder than what is expected for this location based on previously reconstructed SSTs for the northernmost Atlantic. We discuss seasonal bias, recording depth, and appropriate consideration of paleolatitudes, all of which complicate the comparison between SST reconstructions and model output. Thermocline dwelling foraminifera record a larger cooling across the EOT (Eocene 19.0 ± 3.4 °C, Oligocene 14.0 ± 3.1 °C, cooling of 5.2 ± 3.2 °C), than foraminifera from the mixed layer, consistent with an increase in ocean stratification which may be related to the onset or intensification of the Atlantic meridional overturning circulation.

Plain Language Summary

During the Eocene, temperatures on Earth were much warmer than today. It is generally believed that the Antarctic ice sheet first developed around 34 million years ago, during the Eocene–Oligocene transition (EOT). How this change occurred is still widely debated, but it is probably caused by a global drop in CO_2 levels and changes in how the ocean currents distribute heat. Here, we study how water temperatures in the surface of the Atlantic Ocean changed across this event.

We use clumped isotopes—a way of reconstructing the temperature from calcites. They were measured on planktic foraminifera that lived near the surface and at the depth where the temperature remains the same year-round.

We find that the surface waters in the North Atlantic ocean cooled by about 2.2 °C, while the foraminifera that record the deeper layer in the water column cooled by approximately 5.2 °C across the EOT. This cooling is similar to reconstructions from organic biomarkers. However, our absolute temperature reconstructions are much colder than previous estimates. We think that our deeper water temperature reconstructions reflect global cooling, while mixed layer temperatures do not cool as much because a warm water current developed, similar to the Gulf Stream.

1 Introduction

Arguably one of the biggest climate changes in the Cenozoic is the Eocene–Oligocene transition (EOT; ∼34 Ma, lasting ∼500 kyr), which reflects the onset of semi-permanent Antarctic glaciation (see Coxall & Pearson, 2007; Hutchinson et al., 2021; Westerhold et al., 2020, for reviews) The growth of the Antarctic ice sheet coincides with a shift to higher values in both oxygen isotope ratios (δ^{18}O, ∼1 ‰) and carbon isotope ratios (δ^{13}C, ∼0.5 ‰) of benthic foraminifera (e.g., Zachos et al., 2001; Zachos, Dickens, & Zeebe, 2008; Westerhold et al., 2020). This onset was associated with a drop in atmospheric CO_2 from ∼910 to 560 µL/L (approximately 1.6×reduction Hutchinson et al., 2021). The impact of Antarctic ice sheet growth on Northern Hemisphere temperatures is debated (Hutchinson et al., 2021; Liu et al., 2018). In particular, potential contemporaneous changes in the Atlantic meridional overturning circulation (AMOC) may have played an important role in driving water temperature change in the North Atlantic across the EOT (Hutchinson et al., 2019).

In the modern ocean AMOC plays an important role in North Atlantic temperatures due to the associated northward heat transport from lower latitudes. An emerging offset in deep sea oxygen isotope composition between the Atlantic and Pacific ocean after the EOT has been interpreted as an onset of Northern Component Water formation in the North Atlantic (Cramer et al., 2009). Additionally, changes in the benthic foraminifera assemblage as well as an increased isotopic gradient between surface and deep water in the Labrador Sea have been interpreted as AMOC initialization or intensification up 1 Myr prior to the EOT (Borrelli, Cramer, & Katz, 2014; Coxall et al., 2018). An ocean model demonstrated that this onset could be triggered by tectonic Arctic–Atlantic gateway shallowing, which blocked freshwater inflow from the Arctic (Hutchinson et al., 2019). AMOC intensification is expected to influence meridional heat transport, making it relevant to sea surface temperature (SST) development in the North Atlantic.

Most of the available North Atlantic EOT SST reconstructions to date were generated using the organic geochemical proxies Uk'_{37} (Liu et al., 2009, Liu2018) and TEX_{86} (Liu et al., 2009; Śliwińska et al., 2019), which are derived from alkenones produced by haptophytic algae and glycerol dialkyl glycerol tetraether (GDGT) from a.o. the eukaryote genus *Thaumarchaeota*, respectively. Globally, there are only few EOT records available that are calcium carbonate-based: four for $\delta^{18}O_{cc}$ (from molluscs, fish otoliths, and planktic foraminifera Kobashi et al., 2004; Wade et al., 2012; Piga, 2020; Coxall et al., 2018) and Mg/Ca (Bohaty, Zachos, & Delaney, 2012; Lear et al., 2008; Pearson et al., 2007), and only one using clumped isotope thermometry (Δ_{47} Petersen & Schrag, 2015; Hutchinson et al., 2021, for a review of EOT temperature reconstructions). The $\delta^{18}O$ proxy depends on assumptions about the isotopic composition of the sea water. Furthermore, carbonate-based reconstructions such as Mg/Ca and $\delta^{18}O_{cc}$ from e.g., planktic foraminifera are susceptible to early diagenetic overprinting at the sea floor, resulting in "frosty" foraminifera that are cold-biased (Sexton, Wilson, & Pearson, 2006).

However, sites that are clay-rich are able to preserve glassy foraminifera, archiving the original test's formation temperature (Sexton, Wilson, & Pearson, 2006; Sexton & Wilson, 2009). One such site, located on the Newfoundland drift margin, has been shown to preserve Eocene planktic foraminifera particularly well (Leutert et al., 2019).

Here we reconstruct IODP site U1411 mixed-layer and thermocline temperatures across the EOT based on clumped isotope thermometry. We use well-preserved planktic foraminifera that are associated with different depth habitats. Clumped isotope thermometry allows us to generate new temperature constraints for the North Atlantic that are independent from the isotopic composition of the sea water ($\delta^{18}O_{sw}$) for different water depths.

2 Material

2.1 Stratigraphy

Sample material was collected from four target intervals from international ocean discovery program (IODP) Site U1411, located at 41°37.1′N, 49°0′W (Norris et al., 2014) to characterize the development of the EOT in broad terms: i) the Eocene, ii) the late Eocene just before the Earliest Oligocene oxygen isotope step (EOIS), iii) the early Oligocene at the start of the early Oligocene glacial maximum (EOGM), and iv) the Oligocene at the end of the EOGM, or possibly shortly thereafter.

The goal is to establish average temperatures well before and after the EOT to determine the temperature change that would be associated with the rapid δ^{18}O shift that occurs during the EOIS. We use the age model from the Neptune database (Renaudie, Lazarus, & Diver, 2020), which is an adaptation of the shipboard age model (Norris et al., 2014) that is based on biostratigraphic events as well as two paleomagnetic reversals (Figure S3). Modern SSTs (depth of 0 m) near this site (within 0.25° of the site's location) fluctuate between $\sim$9.4 $\pm$ 1.3 °C and 19.5 $\pm$ 0.9 °C seasonally, with an annual average of 13.8 $\pm$ 1.1 °C based on World Ocean Atlas (WOA) data (Locarnini et al., 2019) and are influenced by surface waters from the Labrador Current as well as the Gulf Stream (Figure 1, Figure S16). Beneath the thermocline, approximately at 300 $\pm$ 25 m deep, temperatures remain 8.4 $\pm$ 0.5 °C year-round. Note that when we compare our mixed-layer dwelling foraminifera to modern temperatures, we refer to the estimated dwelling depth of the foraminifera of 50 $\pm$ 25 m instead of SST (see Section 2.2).

2.2 Planktic foraminifera

Foraminifera species were identified based on the framework presented in Holmström (2016). The most abundant planktic foraminifera species that were identified in the samples near the EOT are listed in Table 1. The dwelling depths of extinct species are not well-constrained. Based on extinct foraminiferal carbon and oxygen isotope compositions, the species we study have been previously associated with verious dwelling depths (e.g., Wade et al., 2018). The large number of new δ^{13}C and δ^{18}O measurements allows us to apply the same approach to re-evaluate these dwelling-depth assignments here (Table 1). Based on the Site U1411 data, we assume that the dwelling depths for *Subbotina corpulenta* and *Subbotina projecta* were in the mixed layer, because their δ^{18}O values agree well with *Turborotalia ampliapertura* values rather than with thermocline-dweller *Catapsydrax unicavus* (Figure S5). Isotopic offsets between these species appear to be regionally and/or temporally variable (e.g., in comparison to Wade & Pearson, 2008), and hence assigning a dwelling depth remains problematic. Note, however, that if we use previously associated dwelling depths, we get similar results for the average carbon and oxygen stable isotopes except for a larger uncertainty (Figure S8).

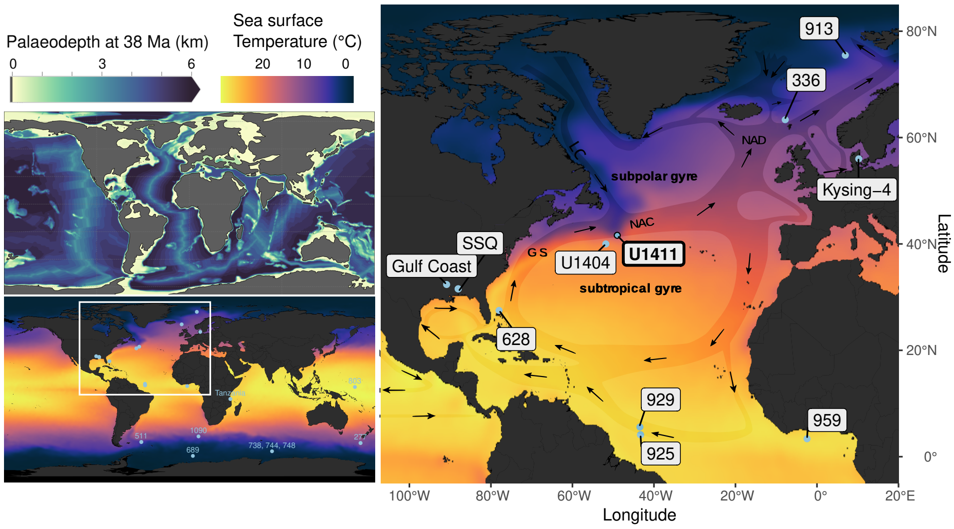

Figure 1. Modern WOA annual mean SST (Locarnini et al., 2019) with site locations for all study sites in the Atlantic (right panel; bottom left panel shows world) (Hutchinson et al., 2021). The global paleobathymetry of Baatsen et al. (2016) is shown in the top left panel. Study site U1411 is located on the Newfoundland margin and in the modern ocean is affected by the Labrador Current (LC) from the North and the Gulf Stream (GS) from the South. This may have been different in the geologic past (see paleobathymetry inset), where the isthmus may have been open, affecting ocean circulation. Ocean current cartoon adapted from De Schepper et al. (2013). NAC = North Atlantic Current, NAD = North Atlantic Drift.

Table 1. Foraminiferal dwelling depths derived from oxygen and carbon isotope compositions (Huber et al., 2016) and their adjustments and simplification in this study. The number of aliquots measured is listed for each of the species and time-periods: Eocene (E), late Eocene (LE), early Oligocene (EO), and Oligocene (O). Note that each number represents roughly 5 to 20 foraminifera tests.

Species	Associated dwelling depth	Assigned depth	E	LE	EO	O	$\sum$	Reference
S. corpulenta	Deep planktonic, subthermocline	Mixed layer	18	48	6	5	77	Wade et a
S. projecta	Thermocline	Mixed layer	12	4		3	19	Wade et a
T. ampliapertura	Shallow, mixed layer, near-surface	Mixed layer	16	13	88	22	139	Pearson et
T. increbescens	Shallow	Mixed layer	3				3	Pearson et
T. cerroazulensis	Shallow subsurface	Mixed layer	5	5	1	2	13	Pearson, F
D. galivasi	Thermocline	Thermocline				2	2	Wade et a
C. unicavus	Thermocline to subthermocline	Thermocline	24	35	48	46	153	Coxall and
C. dissimilis	Subthermocline	Thermocline	4			7	11	Coxall and

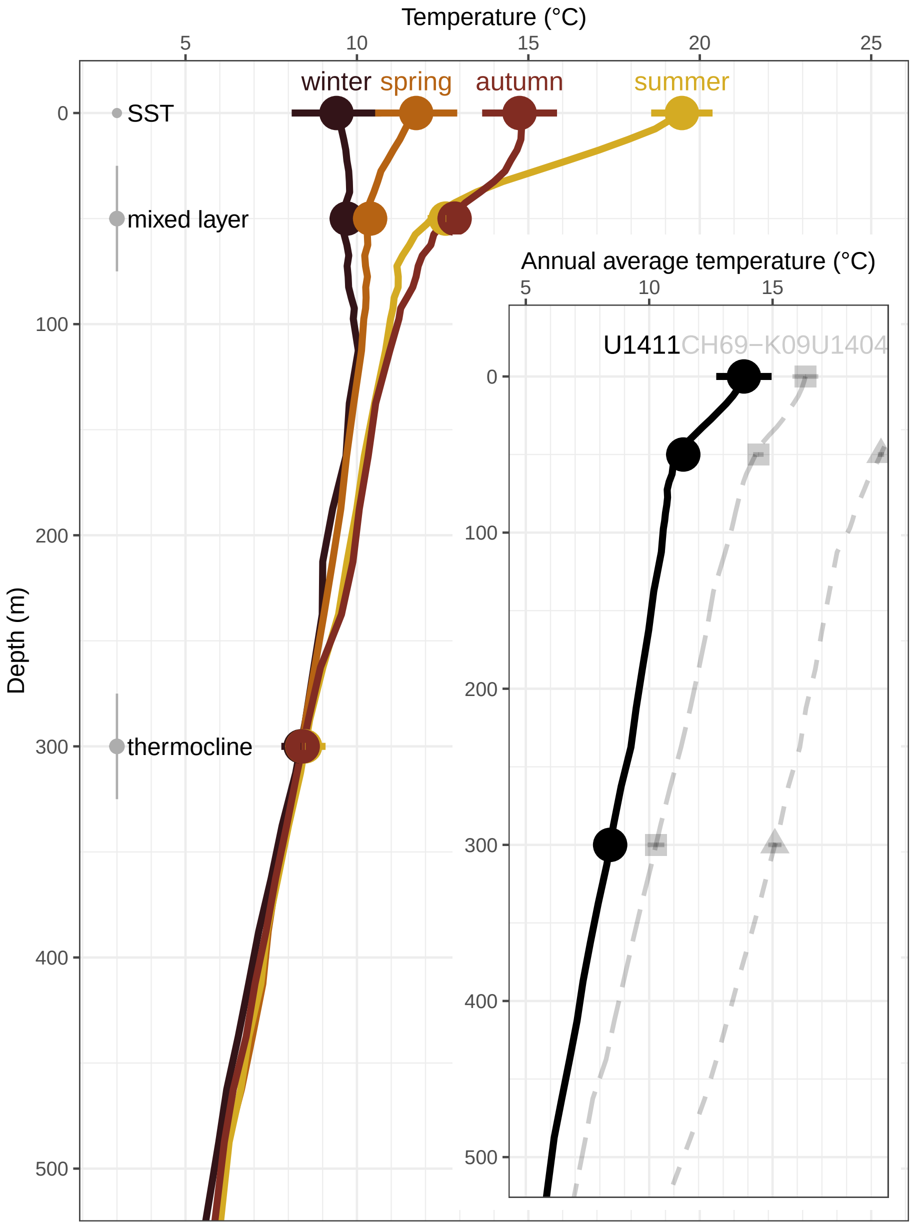

Figure 2. Modern temperature profile of the North Atlantic near site U1411 (this study, average of data within 0.25°) from the WOA (Locarnini et al., 2019). Indicated depth ranges (gray points with bars) represent the assumed thermocline and mixed-layer foraminifera dwelling depths for comparison to modern ocean temperatures. Point estimates with error bars (95% CI of data within 0.25°) indicate the average of the indicated depth interval. The inset shows annual average temperature profiles for sites U1411, site CH69-K09, and site U1404.

Since clumped isotope analysis requires many replicate measurements to get an accurate statistical average value, samples were measured from three size fractions (150 to 250 µm, 250 to 355 µm, and >355 µm). Results derived from the different size fractions were similar and were averaged to provide more replicates and tighter constraints (Figure S12). Based on the similarity between δ^{18}O results before and after the EOT (Figure 4, Figure S4, and Figure S5), thermocline and mixed layer results were averaged separately for the Eocene and for the Oligocene clumped isotope results in order to arrive at more precise temperature estimates.

Foraminiferal $\delta^{18}O_{cc}$ and Δ_{47} data, especially from planktic foraminifera, are sensitive to post-depositional dissolution and re-crystallisation (Pearson et al., 2001). Many planktic foraminifera isotope data from previous studies have had to be discarded as recording recrystallized, non-primary signals. Therefore, we took particular care to select a site with excellent preservation of foraminifera (Leutert et al., 2019). The foraminiferal tests showed original micro-structures and pores and rarely displayed secondary crystals only (Figure 3).

2.3 Modern foraminifera dwelling depths and temperatures

Similar to all biologic water column proxy carriers, planktic foraminifera grow for a limited time, mostly forced by food or nutrient limitations, and they record temperatures of their growing season (e.g., Tolderlund & Bé, 1971). Planktic foraminifera species have a preferred temperature range that they can tolerate (Kucera, 2007), where the species that occur in the midlatitudes tend to have a larger range of tolerance than those in the tropics. Those foraminifera that dwell in the mixed layer are known to calcify mostly during the spring bloom (Ganssen & Kroon, 2000, e.g.,). Dwelling depths of modern planktic foraminifera can be established from plankton hauls at various depths. Some studies indicate that almost no modern foraminifera live in the top 25 m (Rebotim et al., 2017). When comparing our mixed-layer dwelling foraminifera results to modern temperatures in the WOA data, we therefore make the comparison to spring 25 to 75 m deep temperatures instead of annual average SST. The WOA spring mixed-layer temperature at site U1411 is 10.4 ± 0.3 °C. This is fairly similar to the annual average temperature at this depth (which is 11.4 ± 0.4 °C).

The thermocline temperature does not change seasonally, so foraminifera that calcify at this depth reflect an annual average temperature, which, at site U1411 is recorded at a depth of ∼300 m (Figure S16). We filter the WOA data between 275 to 325 m when comparing to our thermocline-dwelling foraminifera, which corresponds to a temperature of 8.4 ± 0.6 °C in the modern ocean. Because we measure many replicates consisting of most of the planktic foraminiferal material in the samples, with enough (≥28) replicates from the different dwelling depths, there is a smaller chance of our results being affected by species-specific caveats.

3 Methods

3.1 Sample preparation

Samples were freeze-dried, washed with deionized water, wet-sieved into 38 to 63 µm, 63 to 150 µm, and >150 µm fractions and dry-sieved into 150 to 250 , 250 to 355 µm and >355 µm fractions. Foraminifera specimens were picked from fraction 250 to 355 µm and >355 µm by species using a Nikon SMZ800 with SCHOTT KL 1500 LCD light source with a painting brush wet with deionized water. Foraminifera were gently crushed between two glass plates and cleaned with deionized water in an ultasonic bath for 20 s. Some samples were prepared at Utrecht University and some at Bergen University. Those that were prepared in Bergen were also rinsed with 200 µL of MeOH prior to ultrasonication. This was not done for all subsequent measurements at Utrecht University since valuable sample material is often lost during the rinsing and there were no visible differences between samples cleaned with or without MeOH. Replicates were weighed between 70 to 95 µg for measurement.

3.2 Microscopy

Color photographs were made using a Keyence VHX-5000 digital microscope. In order to investigate planktonic foraminifera preservation and the efficacy of the cleaning procedure, both cleaned and uncleaned samples were prepared for SEM imaging by placing foraminiferal tests or fragments on a stub with a two-sided carbon sticker and adhering 4 nm of Pt/Pd-target. Images were generated on a JEOL-Neoscope JCM6000 Benchtop SEM. The figure panels in Figure 3 were created by manually cutting out the foraminifera from the background and laying them out in Inkscape (Project, 2021).

All SEM photographs are provided on (**Kocken2022forampics**).

3.3 Clumped Isotope analysis

3.3.1 Measurement

The sample and standard aliquots were measured on a Kiel IV carbonate device modified with a custom-built Porapak trap with a Thermo Fisher MAT 253 plus isotope-ratio mass spectrometer (IRMS) in the laboratories of Utrecht University (UU) and Bergen University (UiB). The method we used was first introduced in Schmid and Bernasconi (2010) and is described in detail in Meckler et al. (2014). In short, samples were dissolved at 70 °C in hypersaturated phosphoric acid (H_3PO_4) in a vacuum. The released gas was purified in two consecutive cold traps interspersed with a manually installed 4 cm Porapak Q bracketed by 1 cm of silverwool kept at −15 °C (Bergen, using Peltier elements) and −40 °C (Utrecht, using a custom-built liquid nitrogen cooling system).

We measured the aliquots in microvolume mode with 40 10 s cycles using the long-integration dual inlet (LIDI) approach (Hu et al., 2014; Müller et al., 2017a).

3.3.2 Carbonate standards

In a single run of measurements, we measured 46 aliquots comprising 20 samples and 26 standards. We used the carbonate standards ETH-1, ETH-2, ETH-3 to convert the measurements to the absolute reference frame (Dennis et al., 2011) with long “sessions” for which we assume that the apparatus is stable. We used the accepted standard values on the I-CDES scale from Bernasconi et al. (2021), who describe carbonate-standardization in detail.

Standards at UiB were measured in equal proportions between ETH-1, ETH-2, ETH-3, and ETH-4 at the time of measurements. At UU, we measured many more ETH-3 standards, since they are much closer to the likely sample Δ_{47} values (Kocken, Müller, & Ziegler, 2019) and allow for intra-run drift correction, dubbed “offset correction” here.

Check standards ETH-4, IAEA-C2, and Merck were measured to establish long-term reproducibility and to monitor the application of the pressure-baseline correction (Bernasconi et al., 2013; He, Olack, & Colman, 2012; Meckler et al., 2014).

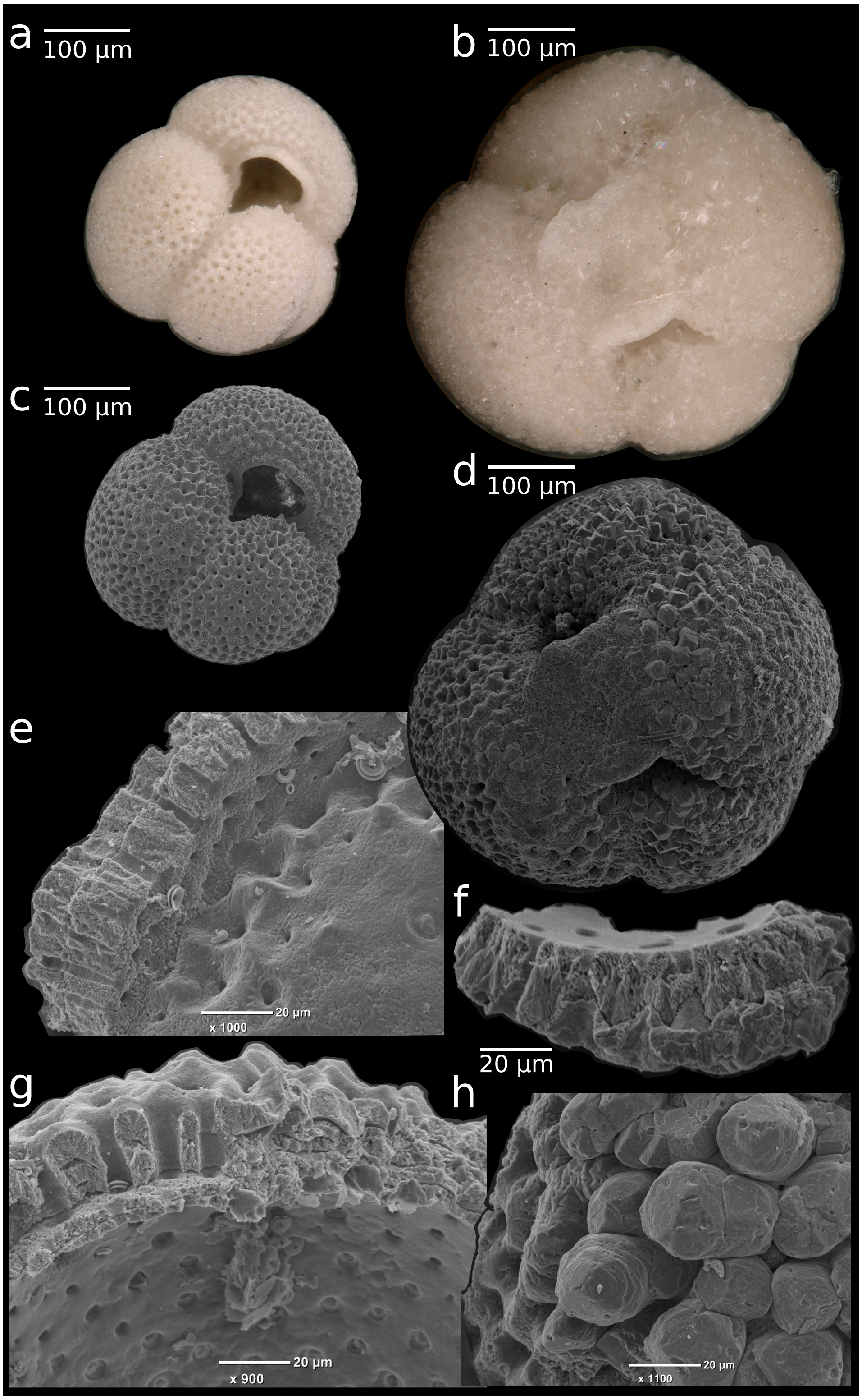

Figure 3. Colour (top row) and SEM photographs (remainder) of *Turborotalia ampliapertura* from sample U1411B 16H5 70 to 72 cm (IK2-010, left column) and *Catapsydrax unicavus* from sample U1411C 5H1 60 to 62 cm (IK1-003, right column). Overall we observed little to no dissolution or recrystallization consistent with Leutert et al. (2019). See **Kocken2022forampics** for all color and SEM pictures.

3.3.3 Data processing

Raw Isodat measurement and scan data were read into memory using the programming language R (R Core Team, 2020) using the package `isoreader` (Kopf, 2020) and processed using `clumpedr` (Kocken, 2019).

We read in the raw measurement files as well as the daily background scans, implemented metadata fixes, additions, and files manually marked as outliers based on machine errors. We calculated the pressure-baseline correction models, which relate local minima in the masses 45 through 49 to the maxima in mass 44 via a 3rd order polynomial (He, Olack, & Colman, 2012; Bernasconi et al., 2013; Meckler et al., 2014). These models were then used to correct the raw intensity data of the measurements scaled by a factor of 0.9 to 1 (for different time periods) for UU and 1 for UiB to minimize the difference between raw ETH-1 and ETH-2 Δ_{47} values (Meckler et al., 2014; Müller et al., 2017b). This is done because we know that the clumped isotope composition of ETH-1 and ETH-2 should be very similar as they were heated at identical elevated temperature conditions to near-stochastic isotope composition, and differences between the two are thus likely the result of uncorrected background effects (Bernasconi et al., 2018).

Measurements with sudden drops in the intensity of the signal (which typically occurs when the previous measurement fails on our Kiel IV device) were automatically (partially, from the drop onward) marked for exclusion when the pressure drop was more than 3× the first cycle drop in pressure. Then, the cycles were summarized for each sample. Samples were marked as failed measurements based on initial mass 44 intensity (below 8 V, greater than 30 V, difference between reference gas and sample gas greater than 3 V).

A rolling offset correction (`expected value − raw value`) was applied within each run to correct for intra-run drift, with a window size of 7 using ETH-3 only for Δ_{47} and a window size of 15 for δ^{18}O and δ^{13}C using ETH-1, ETH-2, and ETH-3.

To correct for scale-compression an empirical transfer function (ETF) was calculated (Dennis et al., 2011), which fits a line to the raw values as a function of accepted standard values (Bernasconi et al., 2021), and applies this conversion in reverse to all raw Δ_{47} data. We used standards ETH-1, ETH-2, and ETH-3 for the ETF, defining three distinct long sessions (Figure S11). The two sessions at UU were defined as 2018-02-23 to 2019-12-21 and from 2020-01-03 to 2021-01-22 and consist of respectively 7859 and

3584 measurements. At UiB, the session ranged from 2018-08-21 to 2018-09-09 and consisted of 405 measurements.

As mentioned earlier, replicate analyses for the two dwelling depths and the four time intervals, as well as pre-EOT and post-EOT were statistically averaged so that a sufficient number of replicates was attained to quantify the uncertainty of the mean value robustly.

3.3.4 Reproducibility of stable isotope measurements

At UU, the $\delta^{13}C$ reproducibility of the independent check standard IAEA C2 was 29.6 and 36.9 ppm (standard deviation, n = 251 and 113) for the two sessions. For $\delta^{18}O$ it was 74.4 and 117.6 ppm and the long-term reproducibility of Δ_{47} was 36.9 and 29.2 ppm.

At UiB, ETH-4 (n = 33) was used as a check standard with standard deviations of 13.1 ppm for $\delta^{13}C$, 40.5 ppm for $\delta^{18}O$ and 37.9 ppm for Δ_{47}.

3.3.5 Temperature calibration

We use the foraminifera calibration from Meinicke et al. (2020), which was recalculated to the I-CDES scale in Meinicke et al. (2021). While it covers a smaller range of formation temperatures than other calibrations, the linear assumption of the regression is more plausible for the smaller interval. An alternative could be the Anderson et al. (2021) calibration, which includes biogenic, abiogenic, and synthetic carbonates and covers a much larger temperature range. However, it appears that at the high temperature range in the Anderson et al. (2021) calibration, the clumped isotope values may be higher than expected from a linear fit. Using the Meinicke et al. (2021) calibration in favor of the Anderson et al. (2021) calibration results in final temperature reconstructions that are $1.520 \pm 0.004\,°C$ warmer (based on the difference for formation temperatures of -5 to $30\,°C$, clumped isotope values between 0.587 to 0.704 ‰ I-CDES, Figure S7). Both calibrations are based on the newest accepted values for the carbonate standards from Bernasconi et al. (2021) that were determinded via heated and equilibrated gases in several laboratories.

Uncertainty from the temperature regression is included in the final temperature estimates via a bootstrapped Monte-Carlo estimation from slope–intercept pairs from

Meinicke et al. (2021, personal communication, re-implemented in R), even though it has a minor influence in the final uncertainty estimates.

3.4 Calculating $\delta^{18}O_{sw}$

The independent temperature estimates from Δ_{47} can be combined with the $\delta^{18}O_{cc}$ values to calculate $\delta^{18}O_{sw}$ values. We do this by solving the quadratic approximation by Kim and O'Neil (1997) as modified by Bemis et al. (1998) for $\delta^{18}O_{sw}$. This is the recommended calibration according to DeepMIP (Hollis et al., 2019).

As such, the isotopic ratio of the seawater ($\delta^{18}O_{sw}$) is calculated by:

$$\delta^{18}O_{swVSMOW} = \frac{16.1 - 4.64\,\delta^{18}O_{ccVPDB} + 0.09\,\delta^{18}O_{ccVPDB} - T}{-4.64 + 0.09}, \tag{1}$$

where T is the temperature in °C, $\delta^{18}O_{cc}$ is in Vienna Pee Dee Belemnite (VPDB), and $\delta^{18}O_{sw}$ is in Vienna Standard Mean Ocean Water (VSMOW).

Uncertainty in the parameters in this equation is ignored in our final $\delta^{18}O_{sw}$ error estimates, as it is poorly constrained and is likely dwarfed by uncertainties in Δ_{47} values.

3.5 Modeling Foraminifera advection

Recent ocean model simulations of the late Eocene (38 Ma) with a higher resolution than usual (0.1deg $compared to$1 deg $orcoarser$, Nooteboom et al., 2021) allow us to use virtual, sinking Lagrangian particles to assess the lateral transport of planktic foraminifera (van Sebille et al., 2015). The small scales that are resolved in these simulations are important to obtain a realistic time-mean flow (Marzocchi et al., 2015; Porta Mana & Zanna, 2014) and eddies, resulting in a representative transport of these virtual particles (Nooteboom et al., 2020). Virtual particles were released every five days for a period of 2 years at the bottom of the ocean in eddying ocean model (0.1° horizontal resolution) of the late Eocene (38 Ma; 2×pCO_2 forcing) with the paleobathymetry of Baatsen et al. (2016) (Figure S1). Each sinking particle was tracked back in time while advected by ocean currents from the ocean bottom until it reached its dwelling depth. Then the particles were tracked back in time at this dwelling depth during their lifespan. This results in a distribution of near-surface foraminifera origin locations, and the temperatures/salinities they experienced during their journey.

We used two distinct dwelling-depths for the foraminifera: the mixed layer foraminifera are assumed to dwell at 50 m deep (Rebotim et al., 2017), while the thermocline and sub-thermocline dwelling foraminifera are modeled at a dwelling depth of 300 m (Groeneveld & Chiessi, 2011). For all planktic foraminifera, the sinking speed was estimated at 200 m/d and they were assigned a life-span of 30 d (Takahashi & Be, 1984). Note that the high sinking speed relative to other sinking particles can be adjusted up or down by up to 100 m/d without affecting the results to a large extent, as advective transport during their life time mostly determines the outcome (van Sebille et al., 2015; Nooteboom et al., 2019).

The site's present-day location was translated to the paleobathymetry with the plate reconstructions of Hinsbergen et al. (2015) using the rotational reference frame of Torsvik et al. (2012) in GPlates (Müller et al., 2018), to determine the site location at 38 Ma. To cope with uncertainties in this paleo-location, a grid of $14° \times 14°$ in both paleolatitude and paleolongitude was generated around the target site to release particles at the ocean bottom. This allows us to test the spatial sensitivity of the backtracking analysis on the paleolatitude/paleolongitude. A total of 28 616 particles were used in one particle backtracking simulation (i.e. for each dwelling depth used).

4 Results

As expected, the planktic $\delta^{18}O$ data were ^{18}O-depleted in comparison to benthic records (Westerhold et al., 2020) but showed a similar amplitude of change across the EOT (Figure 4). Prior to the EOT, the thermocline-dwelling foraminifera showed a similar $\delta^{18}O$ (-0.15 ± 0.08 ‰) value to the mixed-layer dwelling foraminifera (-0.32 ± 0.08 ‰, Figure 4). The $\delta^{18}O$ of the thermocline-dwelling foraminifera increased to 0.17 ± 0.07 ‰ approaching the EOT while the mixed-layer foraminifera changed to -0.19 ± 0.07 ‰. Shortly after the EOT the offset in $\delta^{18}O$ between thermocline-dwellers (1.40 ± 0.10 ‰) and mixed-layer species (0.42 ± 0.06 ‰) increased. In the early Oligocene, the $\delta^{18}O$ of the thermocline-dwelling foraminifera remained offset (1.30 ± 0.18 ‰), while the mixed-layer foraminifera recorded 0.39 ± 0.26 ‰. The $\delta^{13}C$ values are similar between the thermocline-dwellers and the mixed-layer dwellers throughout the record, with the largest offsets (of $\sim$0.14 ‰) just before and after the EOT (Figure 4). On average, the thermocline and mixed-layer δ^{13}C values change from $\sim$0.66 $\pm$ 0.04 ‰ to $\sim$0.81 $\pm$ 0.03 ‰, then increase to $\sim$1.41 $\pm$ 0.03 ‰ across the transition and then decrease again to $\sim$0.78 $\pm$ 0.05 ‰. See Figure S4 for a crossplot of δ^{13}C and δ^{18}O grouped by species.

Absolute δ^{13}C values and changes across the EOT are in agreement with the benthic δ^{13}C data in Westerhold et al. (2020), with the caveat that the composite record is based on the () 2012 (Gradstein et al., 2012) magnetic polarity chron ages as initial age models, which were then tuned to astronomical solutions, whereas our age model is based on biostratigraphic events presented on the tuned GTS 2020 (Speijer et al., 2020). This means that, for example, the subtly lower δ^{13}C values at $\sim$33.75 Ma could be the result of different astronomical tuning options.

We briefly discuss the δ^{13}C results here, because extensive discussion is beyond the scope of this paper. The general agreement between our planktic δ^{13}C data with the benthic record indicates that the carbon cycle perturbation across the EOT represents a global, depth-integrated signal, whereas the δ^{18}O data show a stratified response across the EOT. A uniform shift in δ^{13}C has previously been associated with either a shelf-to-basin carbonate shift with highly ^{13}C-enriched shelf carbonates, or a sequestration of $\sim$1000 Pg of organic carbon via permafrost and peatland expansion during the EOT (Armstrong McKay, Tyrrell, & Wilson, 2016).

Clumped isotope-derived temperature estimates are (20.7 $\pm$ 4.1), (21.3 $\pm$ 4.0), (19.3 $\pm$ 2.3) and (16.6 $\pm$ 5.5) °C (N = 43, 52, 75 and 22, from late Eocene to early Oligocene) for the mixed-layer dwelling foraminifera and (22.3 $\pm$ 4.1), (17.8 $\pm$ 5.3), (12.5 $\pm$ 4.2) and (16.9 $\pm$ 5.2) °C (N = 24, 31, 37 and 28) for the thermocline dwellers (Table S1). When we average the Eocene and the Oligocene temperatures in order to gain more precise estimates, we obtain Eocene SSTs of (21.0 $\pm$ 2.8) and (19.7 $\pm$ 3.5) °C for the mixed layer (N = 95) and the thermocline dwelling species (N = 55) respectively, while Oligocene temperatures were (18.7 $\pm$ 2.2) and (14.4 $\pm$ 3.2) °C (N = 94 and N = 65 respectively), indicating a cooling of (1.8 $\pm$ 2.4) and (5.5 $\pm$ 3.2) °C for the two dwelling depths (Table 2).

The $\delta^{18}O_{sw}$ values for the late-Eocene, pre-EOT, post-EOT, and early-Oligocene are (0.68 $\pm$ 0.81), (0.95 $\pm$ 0.82), (1.10 $\pm$ 0.45) and (0.50 $\pm$ 0.95) ‰ for the mixed layer dwelling foraminifera and (1.20 $\pm$ 0.82), (0.55 $\pm$ 1.10), (0.60 $\pm$ 0.81) and (1.50 $\pm$ 0.97) ‰ for the thermocline-dwelling foraminifera (Figure S6). On average, this results in (0.82 $\pm$ 0.57) and (0.98 $\pm$ 0.40) ‰ for the mixed layer during the Eocene and Oligocene respectively.

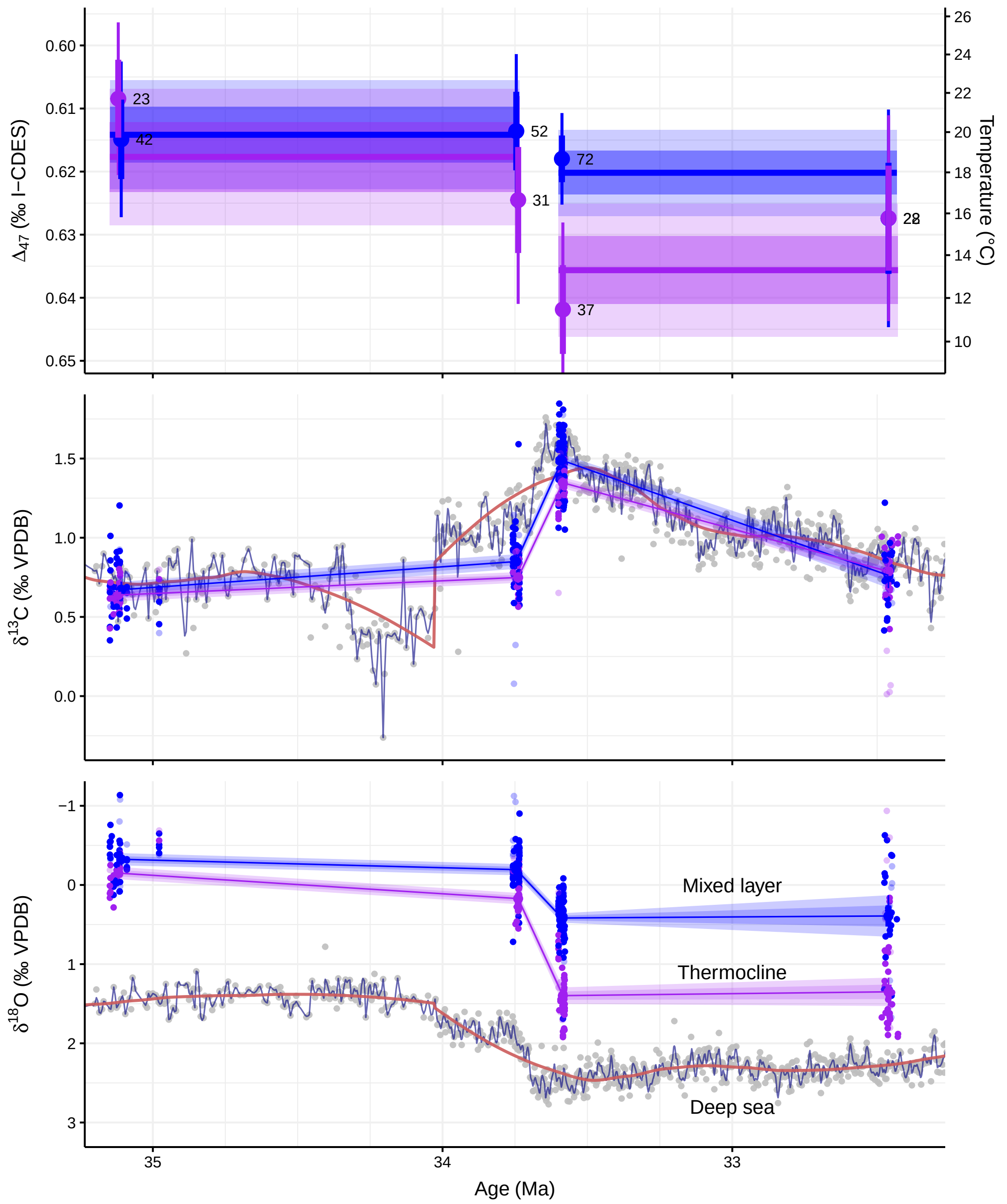

Figure 4. Stable oxygen (δ^{18}O), carbon (δ^{13}C) and clumped (Δ_{47}) isotope composition across the EOT. Clumped isotopes record different amounts of cooling for the mixed layer (blue) and the thermocline (purple). Individual replicates are shown for δ^{13}C and δ^{18}O (points) but not for Δ_{47} because of the large instrumental noise. Replicates that were marked as failed measurements are shown as more transparent points. We show mean ± 68 and 95 % CIs for each time period and dwelling depth (points with thick and thin error bars) as well as late-Eocene and early Oligocene averages (horizontal lines with more or less transparent rectangles). Deep-sea δ^{13}C and $\delta^{18}O_{cc}$ data (gray dots and 1 Myr (red) and 200 kyr (blue) moving averages) are from Westerhold et al. (2020). The temperature axis in the top panel is calculated using the updated foraminifera calibration by Meinicke et al. (2021).

Table 2. Clumped isotope results averaged before and after the EOT (mean ± 95% confidence level). The average age differs between dwelling depths based on the number and spacing of replicates along the core. M = mixed-layer, T = thermocline.

	age	N	δ^{13}C (‰ VPDB)	δ^{18}O (‰ VPDB)	Δ_{47} (‰I−CDES)	T (°C)	$\delta^{18}O_{sw}$ (‰ VPDB)
M	34.4	94	0.77 ± 0.038	-0.25 ± 0.054	0.61 ± 0.0086	21 ± 2.8	0.82 ± 0.57
M	33.3	94	1.3 ± 0.072	0.41 ± 0.075	0.62 ± 0.0068	19 ± 2.2	0.98 ± 0.4
T	34.3	54	0.7 ± 0.029	0.035 ± 0.067	0.62 ± 0.011	20 ± 3.5	0.84 ± 0.7
T	33.1	65	1.1 ± 0.075	1.4 ± 0.096	0.64 ± 0.011	14 ± 3.2	0.99 ± 0.61

For the thermocline, we get (0.84 ± 0.70) and (0.99 ± 0.61) ‰ across the transition. The uncertainties for these values are large because they inherit the uncertainty from the clumped isotope-derived temperatures, rendering it difficult to distinguish instrumental noise from a primary signal (Table S1). However, the overall values may indicate an ^{18}O enriched sea water composition compared to expected values, after taking into account ice-volume effects. In the modern ocean $\delta^{18}O_{sw}$ estimates near site U1411 are around 0 ‰ VSMOW near the surface, increase to 0.26 ± 0.09 ‰ in the mixed layer and to 0.50 ± 0.08 ‰ in the thermocline, and ultimately decrease to 0.260 ± 0.003 ‰ beneath 2000 m (Schmidt, Bigg, & Rohling, 1999).

We show in Figure S6 how the different equations affect the $\delta^{18}O_{sw}$ estimates. They increase the average by up to 0.34 ‰ or decrease it by ∼0.20 ‰, depending on the equation used. All the averages fall approximately within our 68% confidence level as determined from the temperature uncertainties when using our preferred equation.

5 Discussion

With our clumped isotope analyses on mixed layer and thermocline dwelling foraminifera, we provide absolute temperature estimates that are independent of the sea water isotope composition spanning the EOT. This leads to new insights on the extent of cooling and changes in the upper water column stratification in the North Atlantic.

In the following we discuss these temperature reconstructions in the context of modern conditions at the site location, a proximal site during the Late Holocene and the last glacial maximum (LGM), and to previous SST reconstructions of the EOT. Then we discuss how lateral advection may have influenced the site, and how the oceanography may have evolved across the EOT in terms of ocean stratification and Atlantic meridional overturning circulation (AMOC).

5.1 Comparison to the modern SST in the North Atlantic

When comparing climate reconstructions to modern ocean temperatures and, importantly, to paleo-climate simulations, the comparison is typically made to a site's paleolatitude, which changes over geologic timescales due to plate tectonics. In the case of Site U1411, the difference between the modern SST for this latitude (∼41°N) and its reconstructed paleolatitude for the Eocene (∼33°N) bands is ∼6.2 °C (Locarnini et al., 2019). Site U1411 is a prime example demonstrating that a simple comparison of reconstructed conditions at the paleolatitude with a corresponding modern latitudinal average can lead to large biases where very different oceanographic settings are compared. The sediments of Site U1411 have accumulated through drift deposits from the North, so the sedimentary archive could be biased to northward surface conditions (Boyle et al., 2017). The oceanography near Site U1411 is strongly influenced by the bathymetry—in particular the Grand Banks shelf that steers the western intensification of the subtropical and subpolar gyres in the region (Figure 1). Even though the paleolatitude of site U1411 was further to the South, the position with respect to the main bathymetric features was similar and hence the large-scale features of the oceanography, with influence from the North and South, was likely similar to the modern ocean. Advection in the water column may have affected the temperature signal captured by the foraminifera, at least seasonally, via the Gulf Stream and the Labrador Current. This is also confirmed by model simulations (Nooteboom et al., 2021) (see Section 5.4).

In order to compare the reconstructed EOT temperatures with the present day, we argue that the temperatures at the modern site location are a more reasonable reference instead of using the temperatures of a latitude that corresponds to the paleo location. The paleolatitude is situated in a very different oceanographic setting in the modern ocean, with a dominant influence of subtropical gyre currents coming from lower latitudes.

Our temperature reconstructions from Eocene and Oligocene mixed-layer dwelling foraminifera are respectively ∼10.6 °C and ∼8.3 °C warmer than the modern ocean mixed-layer (depth of 50 ± 25 m) spring temperature near site U1411. The Eocene and Oligocene thermocline-dwelling foraminifera at site U1411 reconstruct respectively ∼8.3 and 5.9 °C warmer temperatures than the modern ocean thermocline annual average temperature (depth of 300 ± 25 m, Figure S16). In view of the warm (up to 20 °C) biomarker-based SST reconstructions in the North Atlantic across the EOT (Liu et al., 2018; Śliwińska et al., 2019; Liu et al., 2009) these temperatures appear to be relatively cool. However, we will show in the next sections that the temperatures we reconstruct are reasonable in the context of available reconstructions of atmospheric CO_2 concentrations for this time interval, climate modeling studies, and reconstructed temperature change at the location during the more recent geologic past.

5.2 Comparison to the Late Holocene and last glacial maximum (LGM)

Since the comparison between proxy reconstructions and water column temperatures is complex due to uncertainties in seasonality and depth habitat of the proxy carrier, we also compare our data to subrecent coretop and Holocene planktic foraminifera temperature reconstructions. We assume that they show similar dwelling depths, habitat preferences, and may show similar seasonality preferences. These Holocene reconstructions are based on Mg/Ca and δ^{18}O and are considered reliable because they are based on well-preserved foraminiferal tests and well-constrained ocean composition for these time periods.

Core-top data from site CH69-K09 (located ∼138 km East of Site U1411 with a slightly offset temperature profile, Figure S16) from *G. bulloides* Mg/Ca indicate 12.3 °C (Riveiros et al., 2016), while *G. inflata* δ^{18}O data from the same site imply 12.8 and 12.3 °C (Cléroux et al., 2008, for two size-fractions). These temperatures are also consistent with an interpretation that the foraminifera capture an average spring temperature of around 50 m deep (which is 10.4 ± 0.3 °C in the modern ocean). Thus, in comparison to site CH69-K09, our late Eocene and early Oligocene mixed-layer dwelling planktic foraminifera temperature reconstructions are respectively ∼8.5 and 6.2 °C warmer.

To put the temperature change at Site 1411 across the EOT into perspective, we further make a comparison with the temperature change that occurred at this location across the last deglaciation starting at the LGM 20,000 years ago. Tierney et al. (2020a) reconstructed LGM (23 to 19 ka) temperatures of 7.8 ± 0.5 °C, based on a proxy ensemble (δ^{18}O, Mg/Ca, Uk'_{37}, and TEX_{86}) combined with an isotope-enabled climate model. They record a difference of 5.6 ± 1.4 °C between the Late Holocene and the LGM. The cooling we observe across the EOT in the thermocline ($5.4 \pm 3.3\,°C$) is similar in magnitude to the warming that occurred between the LGM and Late Holocene SST. Without discussing potential implications on climate sensitivity in great detail, we note that when comparing these changes simply with associated changes in atmospheric CO_2, our results show a consistent pattern at this location: we record similar cooling between a warmhouse, ice-free world, and a coolhouse with a permanently glaciated Antarctica (using the terminology from Westerhold et al., 2020) with a 1.58-fold CO_2 decrease (from 885 to 560 ppm Hutchinson et al., 2021) compared to a 1.56-fold increase (~180 to 280 ppm) and associated warming from LGM to Late Holocene (Tierney et al., 2020a).

5.3 Absolute clumped-isotope based EOT temperatures were cooler than previous North Atlantic reconstructions

Eocene organic proxy records reconstruct warm sea surface temperature (SST) from Atlantic mid-to-low paleolatitudes (10 to 40°N, $\sim 27.0 \pm 3.2\,°C$, mean ± 95% CI assuming independent errors). The organic proxies also reconstruct warm high latitudes for the North Atlantic. For Kysing-4, located at 50.3°N, TEX_{86} data indicate $24.0 \pm 2.7\,°C$ Śliwińska et al. (2019). Site 336 and 913, located at 56.4 and 67.5°N, Uk'_{37} data reconstruct (20 ± 2) and $(18.2 \pm 2.2)\,°C$ Liu et al. (2009). See Hutchinson et al. (2021) for a review and Figure 5.

In comparison to the North Atlantic values, our mixed-layer clumped isotope temperatures from Site U1411 are cooler by about 0.71 °C during the Eocene and by ~1.3 °C during the Oligocene, although our sampling site is located much farther to the South (Figure 5). Śliwińska et al. (2022) recently reconstructed southern Labrador Sea (ODP Site 647, latitude of 53°20′N) EOT temperatures of (26.4 ± 0.5) to $(24.3 \pm 0.3)\,°C$ (Eocene and Oligocene values calculated from their raw data). Their temperature estimates were ~5.5 and 5.7 °C warmer than our mixed layer reconstructions for the Eocene and Oligocene respectively (~6.7 and 9.9 °C warmer than our thermocline reconstructions).

IODP Site U1404 is the closest site for which EOT temperature reconstructions are available. It is located ~297 km South West of U1411 and was analyzed by Liu et al. (2018) using Uk'_{37}. Their temperature reconstructions for the latest Eocene are warmer by ~7.2 °C compared to our estimates for the thermocline and mixed-layer. At the beginning of the Oligocene, Site U1411's mixed layer foraminifera are ~7.7 °C cooler than temperature reconstructions for site U1404. In the modern ocean, the temperature difference between sites U1404 and U1411 is $\sim$8.0 °C at 50 ± 25 m deep and 6.7 °C at 300 ± 25 m (Locarnini et al., 2019, Figure S16), which is similar in magnitude to our observed differences. Therefore, our findings could be compatible with those of site U1404 if we assume that the oceanography was comparable to the modern during the EOT—the subpolar- and subtropical gyre circulated in the same direction—and that the Uk'_{37} proxy represents a surface or mixed-layer signal (Liu et al., 2018). However, if we extend the comparison to proxy records farther to the north of our study site and consider the reconstructions for the southern Labrador Sea (Śliwińska et al., 2022), it appears that the organic proxies capture systematically warmer temperatures than our clumped isotope results (Figure 5). This may have implications for the proxy–model mismatch, where Eocene models are unable to reproduce the low meridional temperature gradient that is inferred from organic proxy records (Huber & Caballero, 2011; Hutchinson et al., 2018).

While the offset in absolute temperatures is very large between our reconstructions and those from higher latitudes made with different proxies, the *change* across the EOT is similar, specifically in comparison to the mixed-layer dwelling foraminifera (Figure 5). The North Atlantic sites Kysing-4, Site 336, and Site 913 record a cooling of $\sim(4.6 \pm 2.7)$, (3.6 ± 2.0) and (4.6 ± 3.8) °C respectively. At Site U1404, a cooling of $\sim$2 °C was recorded (Liu et al., 2018), while Site 647 showed a cooling of $\sim 2.1 \pm 0.5$ °C (Śliwińska et al., 2022, calculated from raw data) across the EOT. This is similar to our mixed-layer foraminifera cooling of $\sim 2.3 \pm 2.2$ °C (Figure 5) across the EOT.

Our temperature change is also similar in magnitude compared to other calcite-based proxies, such as Mg/Ca from Tanzania (paleolatitude of 16.59°S), which records 1.1 °C cooling (Lear et al., 2008) and from ODP sites 738, 744 and 748 (paleolatitude of 56.7°S) with 2.6 °C cooling (Bohaty, Zachos, & Delaney, 2012). δ^{18}O-based reconstructions from the Gulf Coast (paleolatitude of 28.5°N) indicate 0.6 °C cooling (Kobashi et al., 2004), while St. Stephens Quarry (SSQ) (paleolatitude of 27.2°N) records only 0.2 °C cooling (Wade et al., 2012; Piga, 2020). However, these estimates have a larger uncertainty due to an unknown contribution of potential changes in $\delta^{18}O_{sw}$ to the signal.

5.3.1 Challenges in comparing SSTs of different proxies

When inferring a latitudinal temperature gradient from specific sites, one needs to take into account potential biases of these site locations with respect to their latitudinal band. Most of the higher-latitude sites are located closer to paleoshorelines, and many of the reconstructions are by necessity derived from semi-enclosed and shallow epeiric seas, potentially leading to warm biases in their SST estimates (Judd, Bhattacharya, & Ivany, 2020) (Figure 1).

As we compare our temperature estimates to those based on different proxies, we briefly discuss the arising challenges. The Uk'_{37} data for this interval show strongly fluctuating concentrations of alkenones—often below the required limit (Liu et al., 2018). Low alkenone concentrations have been associated with warm-biases caused by chromatographic irreversible absorption (Grimalt, Calvo, & Pelejero, 2001). Many Uk'_{37} data also exhibit saturation of the index (Liu et al., 2018), which is thought to occur above 29 °C (Brassell et al., 1986). This would, however, result in a bias to cooler than 29 °C temperatures. Furthermore, the data in the compilation rely on the Prahl, Muehlhausen, and Zahnle (1988) calibration, which has been shown to have very warm residuals in the North Atlantic (Tierney & Tingley, 2018). This is likely due to sea ice effects and a general summer and fall bias in the North Atlantic on Uk'_{37}, and while these issues likely did not affect the site to the same extent near the EOT, using these data for the calibration may introduce additional uncertainty.

Some of the challenges with the TEX_{86} proxy are contamination of the target signal with terrestrial inputs of GDGTs, *Euriarchaeota*—which contribute to the GDGT pool through anaerobic oxidation of methane—and, if the *Thaumarchaeota* do contribute significantly to the GDGT pool, potential bias towards summer temperatures. While these issues are largely addressed by the original authors, as well as in later data compilations (Inglis et al., 2015), the production depth of the GDGTs remains disputed. The GDGTs are likely produced in the shallow subsurface (50 to 300 m) while they were calibrated to the sea surface (see Ho & Laepple, 2016; Tierney et al., 2017; Ho & Laepple, 2017; Zhang & Liu, 2018; Tierney et al., 2020b, for discussion). A potential solution to monitor whether GDGT production occurred at depth has recently been presented in a preprint (van der Weijst et al., 2021), and we will see how this affects future TEX_{86} studies.

The changing Δ_{47} offset that we record between the mixed-layer dwelling foraminifera and the thermocline-dwelling foraminifera demonstrates that one ought to be careful when using subsurface temperature signals to reconstruct SST. Ocean stratification is spatially heterogeneous and the relationship between the subsurface and the surface, while strong, does not necessarily hold over geologic time and is often variable for modern ocean sites. Production of GDGTs at greater depth may play a small but significant role in the final TEX_{86} signal recorded in the sediment. Therefore it is difficult to assess how the TEX_{86} signal could be affected by changes in stratification through time. Applying a core-top TEX_{86} calibration to modern subsurface temperatures would result in colder reconstructed palaeotemperature estimates with smaller variability, which would be in better alignment with model results for latitudinal temperature gradients (Ho & Laepple, 2016).

We do have to consider the potential effects of diagenetic overprinting on our clumped isotope record, as planktic foraminifera were previously shown to be sensitive to diagenetic overprinting of the $\delta^{18}O$ signal (Sexton, Wilson, & Pearson, 2006). However, the foraminifera at the Newfoundland Margin are generally well-preserved (Leutert et al., 2019). We calculated the extent of diagenetic overprinting required to arrive at our clumped isotope temperatures under several scenarios of bottom water temperatures and true SST (further discussed in Section S8.1 and illustrated in S2) and find that under the worst-case scenario—a warm true SST of $\sim$20 °C with cold bottom water temperatures of 0.0 °C for maximum overprinting effect—record would require >10 % overprinting, which, from the SEM and light microscope images (Figure 3) and previous studies (Leutert et al., 2019) seems unlikely. Some diagenetic overprinting of the formation temperature cannot be excluded from SEM images alone, and thus our results could be biased towards cooler temperatures captured in the bottom waters and during early diagenesis in the sediment.

5.4 Lateral advection

Site U1411 is a sediment drift deposited during the EOT, so temperature reconstructions are likely biased to foraminifera that sank to the North of the site and have been laterally transported (Boyle et al., 2017). Liu et al. (2018) argue why lateral transport is unlikely to have played a major role for site U1404, which is close to our study site U1411. First, they note that in the modern ocean there is only an insubstantial difference ($\sim$1.1 °C) between alkenone-based temperatures from surface waters and the sea

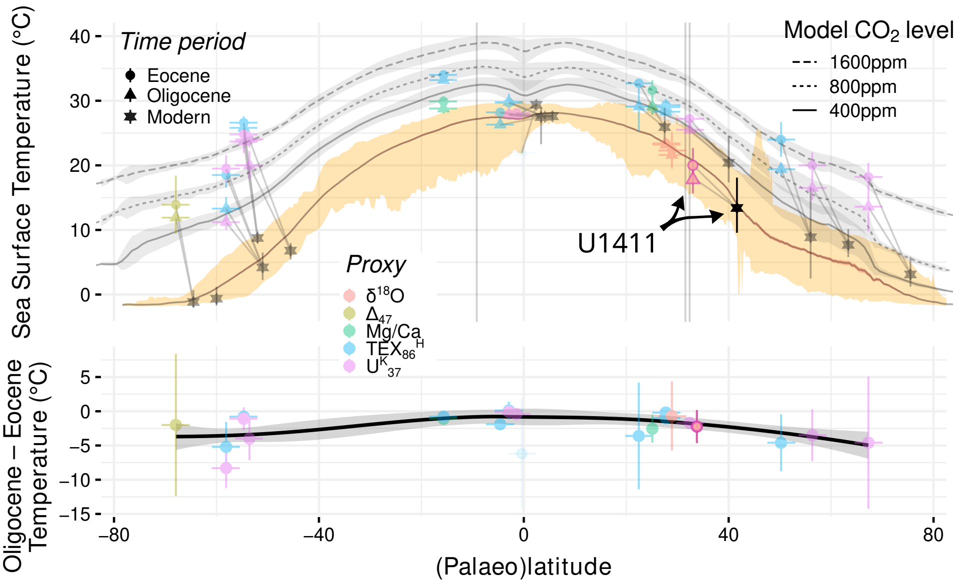

Figure 5. SST estimates as a function of (paleo)latitude (top panel) for the various proxy records available (colors) (Hutchinson et al., 2021). The modern SST variability is indicated as the annual average (line, red shading is the 95% CI, very narrow) and the full range (yellow shaded interval), as well as for the different sites (black square and range, vertical gray lines for modern site locations that have no modern ocean temperature in the WOA) (Locarnini et al., 2019). Eocene (circles) and Oligocene (triangles) temperature estimates show warmer temperatures at higher latitudes due to polar amplification. Note that a simple comparison of site U1411 EOT reconstructions to the modern temperatures at the site's paleolatutide does not reflect the nuanced context of these changes, because the North Atlantic basin was more restricted (Figure 1) with implications for the oceanography. The 3 model outputs with different levels of CO_2 forcing (1600 ppm = dashed, 800 ppm = dotted, and 400 ppm = continuous line, all with gray shading) by Hutchinson et al. (2018) illustrate how models cannot reconcile very high polar temperatures with relatively cool tropical temperatures. The cooling across the EOT (bottom panel) is larger at higher latitudes. Horizontal error bars represent the 95% confidence interval of the paleolatitude reconstruction for 34 Ma. Vertical error bars in the top panel represent uncertainties as presented in Hutchinson et al. (2021). In the bottom panel, we recalculated the uncertainties as the mean squared error of the difference. The error bars for our new Site U1411 datapoint represents the 95% confidence interval and the 95% confidence interval of the difference.

floor in comparison to directly measured SST. Second, that a latitudinal temperature gradient exists for their alkenone-based reconstructions between their site and sites 336 and 913, which are located further North. Last, their reconstructed minimal cooling across the EOT is incompatible with transport from the North, which would occur due to the influence of the deep western boundary current.

Lateral advection in the water column, however, cannot be excluded. It likely influenced how both haptophytic algae and foraminifera were transported to ultimately arrive at the sites. In the late Eocene (38 Ma) eddying OGCM simulations (Nooteboom et al., 2021) a midlatitude gyre exists, with a northeastward flowing Gulf Stream. However, the mid-latitude gyre circulates less intensely in these simulations compared to the present-day, likely because the Atlantic basin was more restricted.

The particle advection simulations in the eddying ocean model indicate that the foraminifera were advected by at most 3.3° southward and 2.6° northward near the study site, which indicates that the temperatures they experienced during their lifetime may originate from between 36.2°N and 30.5°N and from 39.7°E and 29.6°E (transported by 5.3° West or 4.8° East; Figure S13). In the modern ocean, mixed-layer temperatures 3.3° northwards of site U1411 are 9.7 °C cooler than above site U1411, while temperatures at 300 m depth are 4.8 °C cooler (Locarnini et al., 2019). Even at 300 m depth we see particle transport of more than 4° west during the simulated particles' 30 day life cycle. Furthermore, foraminifera dwelling above site U1404 may end up on site U1411, and vice-versa (Figure S13, Figure S15).

We have to consider that these simulations do not account for foraminifera habitat preferences, however. That is to say, the particle back-track analysis only depends on the ocean currents. In reality, planktic foraminifera have preferred habitats, such as ranges of temperatures that they can tolerate, as well as for salinity and pH (Nooteboom et al., 2019). For example, it could be that cold eddies from the north are always void of foraminifera, and therefore foraminifera-based reconstructions result in a different final temperature signal from what is modeled.

On average, however, the particles suspended directly above Site U1411 captured very similar temperatures to those that finally ended up in the sediments of Site U1411 in the simulations. This finding is consistent with temperature reconstructions based on modern and Holocene foraminifera around the site agreeing with observed mixed layer temperatures. All of our temperature data (Figure 4) are based on many different foraminifera (each datapoint is made up of at least 22 aliquots, each consisting of at least ∼80 µg, so at the very least 100 foraminifera per datapoint), and are thus very likely to capture an average temperature representative of the site's location.

5.5 Increased ocean stratification

Our $\delta^{18}O$ and Δ_{47} results show that during the latest Eocene, both mixed-layer- and thermocline dwelling foraminifera record similar water masses. Towards the Oligocene this changes, with thermocline-dwelling species recording much colder temperatures and higher $\delta^{18}O_{cc}$ values (Figure 4). For Site U1411, this could indicate an adjustment of the growing season of the surface dwellers or a change in water column stratification. Because at least some of the species (e.g., *T. ampliapertura* and *C. unicavus*) occur throughout the record as some of the most abundant species, we think that the change in recorded mixed layer and thermocline temperature is likely the result of changes in ocean stratification of the upper water column.

5.5.1 What could our records mean for AMOC?

The observed changes in North Atlantic stratification may be related to AMOC intensity, which is thought to have initiated around 1 to 0.5 Myr prior to the EOT (Cramer et al., 2009; Borrelli, Cramer, & Katz, 2014; Coxall et al., 2018, i.e. shortly after our oldest datapoint). The onset of the AMOC may be compatible with our record, where we see some increased stratification prior to the EOT (between our oldest and second-oldest datapoint) with subsequent intensification of the AMOC leading to more pronounced stratification between the thermocline and the mixed layer across the EOT. The offset in timing could also be the result of different age models, but this is unlikely around an event such as the EOT that is relatively easy to find in a record. Changes in AMOC strength have a strong influence on the heat transport in the North Atlantic region. With a stronger AMOC, heat transport intensifies in the mixed layer via the Gulf Stream and North Atlantic Drift from the lower latitudes to the higher Northern latitudes. As a consequence of such an AMOC intensification, ocean stratification could have been amplified by increased influence of southern-sourced Gulf Stream waters on the mixed layer.

One potential mechanism for the AMOC initiation prior to the EOT was proposed by Hutchinson et al. (2019). They argue that during the late Eocene, some fresh water from the Arctic ocean entered the North Atlantic via the shallow Fram Strait connection. This inflow of low-salinity waters prevented deep-water formation in the North Atlantic. Around the EOT, tectonic closure of the Arctic–Atlantic gateway may have blocked freshwater inflow from the Arctic, resulting in the increased salinity in the North Atlantic and deep water formation at high northern latitudes, leading to AMOC onset or intensification. The warm salt waters from the mid-latitudes were transported farther to the north, warming the region with respect to the Pacific. If restricted to the surface, these warm salty waters could have led to an increased stratification at Site U1411, with a cooler thermocline than the surface waters at this site. In the northern North Atlantic, this Arctic–Atlantic gateway closing caused increased mixed layer depth, but this was limited to areas north of our study site in the model simulation (Hutchinson et al., 2019, supplementary figure 3).

Model simulations demonstrate that the North Atlantic subsurface responds differently to changes in AMOC intensity compared to the surface ocean (Śliwińska et al., 2022). For the surface ocean, weakening of AMOC reduces the transport of warm waters from lower latitudes towards the northern Atlantic, leading to a bipolar seesaw behavior in the temperature response (Liu et al., 2009). The subsurface ocean however exhibits warming throughout the Atlantic ocean in response to a suppressed convective heat exchange in the North Atlantic. This temperature response has been studied in detail using models and reconstructions across the last deglaciation, when large scale changes in AMOC intensity occurred.

The pronounced cooling of the thermocline dwelling foraminifera across the EOT can be related to an onset of AMOC across the transition in combination with a global cooling across the boundary. While the mixed layer ocean at site U1411 is relatively insensitive to AMOC changes (Śliwińska et al., 2022, figure 6), the observed cooling across the EOT can be largely ascribed to the global cooling associated with a reduction in atmospheric CO_2. The subsurface cooling instead is likely amplified through the combined effects of a global scale cooling across the EOT as well as an intensification of the AMOC across the event related to a contemporaneous closure of the connection between Arctic and North Atlantic.

5.6 Conclusions

We present the first clumped isotope based surface ocean temperatures across the EOT in the North Atlantic region using well-preserved planktic foraminifera from IODP Site U1411. Importantly, we find a larger cooling in the subsurface compared to the surface reconstructions, which is consistent with a scenario in which global cooling associated with a drop in atmospheric CO_2 is accompanied by an onset of the AMOC due to tectonic restrictions in the connections between the Arctic and the North Atlantic.

Earlier studies that have used organic-geochemical proxies to derive SSTs arrive at significantly higher temperatures, which appear inconsistent with modeling simulations. We argue that such differences may originate through various non-thermal influences on the different proxies; for example a different production depth for TEX_{86} records.

6 Acknowledgements

This work is part of the NWO VIDI project 016.161.365, which is financed by the Netherlands Organization for Scientific Research (NWO). Analyses at the UiB were possible through funding from the Bjerknes Centre for Climate Research through a fast track intiative grant to Petra Langebroek. ANM acknowledges funding from the European Research Council (project number 638467). IJK acknowledges Arnold van Dijk for laboratory assistance. The code used to process clumped isotope results from machine output to final clumped values is distributed under the GPL-3 license and is available in `https://github.com/UtrechtUniversity/clumped-processing` **TODO** (will be made available upon publication). The code used to calculate sample averages and create the figures is available in **TODO** (will be made available upon publication). All clumped isotope replicate data have been uploaded to the EarthChem database under **TODO**. The code used for the back-tracking analysis is distributed under the MIT license and can be found at the website `https://github.com/pdnooteboom/NA\_forams` (will be assigned a DOI upon publication). Model output and boundary conditions such as the bathymetry can be found on YODA: `https://doi.org/10.24416/UU01-AYNLZP`. PN acknowledges support from the Netherlands Organization for Scientific Research (NWO), Earth and Life Sciences, through project ALWOP.207. The use of the SURFsara computing facilities was sponsored by NWO–EW (Netherlands Organisation for Scientific Research, Exact Sciences) under the project 15508.

7 References

Anderson, N. T. et al. (2021). “A Unified Clumped Isotope Thermometer Calibration (0.5–1100°C) Using Carbonate-Based Standardization”. In: *Geophysical Research Letters* n/a.n/a, e2020GL092069. DOI: 10 .1029 / 2020GL092069 (cit. on pp. 13, 46).

Armstrong McKay, David I., Toby Tyrrell, and Paul A. Wilson (Feb. 2016). “Global Carbon Cycle Perturbation across the Eocene-Oligocene Climate Transition”. In: *Paleoceanography* 31.2, pp. 311–329. DOI: 10.1002/2015PA002818 (cit. on p. 16).

Baatsen, Michiel et al. (Aug. 2016). “Reconstructing Geographical Boundary Conditions for Palaeoclimate Modelling during the Cenozoic”. In: *Climate of the Past* 12.8, pp. 1635–1644. DOI: 10.5194/cp-12-1635-2016 (cit. on pp. 6, 14, 40).

Bemis, Bryan E. et al. (1998). “Reevaluation of the Oxygen Isotopic Composition of Planktonic Foraminifera: Experimental Results and Revised Paleotemperature Equations”. In: *Paleoceanography* 13.2, pp. 150–160. DOI: 10.1029/98PA00070 (cit. on pp. 14, 45).

Bernasconi, S.M. et al. (Apr. 2021). “InterCarb: A Community Effort to Improve Interlaboratory Standardization of the Carbonate Clumped Isotope Thermometer Using Carbonate Standards”. In: *Geochem Geophys Geosyst.* DOI: 10.1029/2020GC009588 (cit. on pp. 10, 12, 13).

Bernasconi, Stefano M. et al. (2013). “Background Effects on Faraday Collectors in Gas-Source Mass Spectrometry and Implications for Clumped Isotope Measurements”. In: *Rapid Communications in Mass Spectrometry* 27.5, pp. 603–612. DOI: 10.1002/rcm.6490 (cit. on pp. 10, 12).

Bernasconi, Stefano M. et al. (2018). “Reducing Uncertainties in Carbonate Clumped Isotope Analysis Through Consistent Carbonate-Based Standardization”. In: *Geochemistry, Geophysics, Geosystems* 0.0. DOI: 10.1029/2017GC007385 (cit. on p. 12).

Bohaty, Steven M., James C. Zachos, and Margaret L. Delaney (Feb. 2012). “Foraminiferal Mg/Ca Evidence for Southern Ocean Cooling across the Eocene–Oligocene Transition”. In: *Earth and Planetary Science Letters* 317–318, pp. 251–261. DOI: 10.1016/j.epsl.2011.11.037 (cit. on pp. 4, 22).

Borrelli, Chiara, Benjamin S. Cramer, and Miriam E. Katz (2014). “Bipolar Atlantic Deepwater Circulation in the Middle-Late Eocene: Effects of Southern Ocean Gateway

Openings". In: *Paleoceanography* 29.4, pp. 308–327. DOI: 10.1002/2012PA002444 (cit. on pp. 3, 27).

Boyle, Patrick R. et al. (Mar. 2017). "Cenozoic North Atlantic Deep Circulation History Recorded in Contourite Drifts, Offshore Newfoundland, Canada". In: *Marine Geology* 385, pp. 185–203. DOI: 10.1016/j.margeo.2016.12.014 (cit. on pp. 19, 24).

Brassell, S. C. et al. (Mar. 1986). "Molecular Stratigraphy: A New Tool for Climatic Assessment". In: *Nature* 320.6058, pp. 129–133. DOI: 10.1038/320129a0 (cit. on p. 23).

Cléroux, Caroline et al. (Apr. 2008). *Mg/Ca and Sr/Ca Ratios of Planktonic Foraminifera from North Atlantic Surface Sediments.* DOI: 10.1594/PANGAEA.832178 (cit. on p. 20).

Coxall, Helen K and Silvia Spezzaferri (2018). "Taxonomy, Biostratigraphy, and, Phylogeny of Oligocene Catapsydrax, Globorotaloides and Protentelloides". In: *Cushman Foundation Special Publication* 4.46, pp. 79–124 (cit. on p. 6).

Coxall, Helen K. and P.N. Pearson (Dec. 2007). "The Eocene–Oligocene Transition". In: *Deep-Time Perspectives on Climate Change: Marrying the Signal from Computer Models and Biological Proxies.* Ed. by M. Williams et al. First. The Geological Society of London on behalf of The Micropalaeontological Society, pp. 351–387. DOI: 10.1144/TMS002.16 (cit. on p. 3).

Coxall, Helen K. et al. (Mar. 2018). "Export of Nutrient Rich Northern Component Water Preceded Early Oligocene Antarctic Glaciation". In: *Nature Geoscience* 11.3, pp. 190–196. DOI: 10.1038/s41561-018-0069-9 (cit. on pp. 3, 4, 27).

Cramer, B. S. et al. (Dec. 2009). "Ocean Overturning since the Late Cretaceous: Inferences from a New Benthic Foraminiferal Isotope Compilation: BENTHIC ISOTOPE COMPILATION". In: *Paleoceanography* 24.4. DOI: 10.1029/2008PA001683 (cit. on pp. 3, 27).

De Schepper, Stijn et al. (Dec. 2013). "Northern Hemisphere Glaciation during the Globally Warm Early Late Pliocene". In: *PLoS One* 8.12. DOI: 10.1371/journal.pone.0081508 (cit. on p. 6).

Dennis, Kate J. et al. (Nov. 2011). "Defining an Absolute Reference Frame for 'clumped' Isotope Studies of CO_2". In: *Geochimica et Cosmochimica Acta* 75.22, pp. 7117–7131. DOI: 10.1016/j.gca.2011.09.025 (cit. on pp. 10, 12).

Erez, Jonathan and Boaz Luz (June 1983). "Experimental Paleotemperature Equation for Planktonic Foraminifera". In: *Geochimica et Cosmochimica Acta* 47.6, pp. 1025–1031. DOI: 10.1016/0016-7037(83)90232-6 (cit. on p. 45).

Ganssen, G. M. and D. Kroon (May 2000). "The Isotopic Signature of Planktonic Foraminifera from NE Atlantic Surface Sediments: Implications for the Reconstruction of Past Oceanic Conditions". In: *Journal of the Geological Society* 157.3, pp. 693–699. DOI: 10.1144/jgs.157.3.693 (cit. on p. 8).

Gradstein, Felix M. et al. (Sept. 2012). *The Geologic Time Scale 2012*. Elsevier (cit. on p. 16).

Grimalt, Joan O., Eva Calvo, and Carles Pelejero (2001). "Sea Surface Paleotemperature Errors in UK′ 37 Estimation Due to Alkenone Measurements near the Limit of Detection". In: *Paleoceanography* 16.2, pp. 226–232. DOI: 10.1029/1999PA000440 (cit. on p. 23).

Groeneveld, Jeroen and Cristiano M. Chiessi (2011). "Mg/Ca of Globorotalia Inflata as a Recorder of Permanent Thermocline Temperatures in the South Atlantic". In: *Paleoceanography* 26.2. DOI: 10.1029/2010PA001940 (cit. on p. 15).

He, Bo, Gerard A. Olack, and Albert S. Colman (2012). "Pressure Baseline Correction and High-Precision CO_2 Clumped-Isotope (Δ_{47}) Measurements in Bellows and Micro-Volume Modes". In: *Rapid Communications in Mass Spectrometry* 26.24, pp. 2837–2853. DOI: 10.1002/rcm.6436 (cit. on pp. 10, 12).

Hinsbergen, Douwe J. J. van et al. (June 2015). "A Paleolatitude Calculator for Paleoclimate Studies". In: *PLOS ONE* 10.6, e0126946. DOI: 10.1371/journal.pone.0126946 (cit. on p. 15).

Ho, Sze Ling and Thomas Laepple (Aug. 2016). "Flat Meridional Temperature Gradient in the Early Eocene in the Subsurface Rather than Surface Ocean". In: *Nature Geoscience* 9.8, pp. 606–610. DOI: 10.1038/ngeo2763 (cit. on pp. 23, 24).

— (Aug. 2017). "Reply to 'Eocene Temperature Gradients'". In: *Nature Geoscience* 10.8, pp. 539–540. DOI: 10.1038/ngeo2998 (cit. on p. 23).

Hollis, Christopher J. et al. (July 2019). "The DeepMIP Contribution to PMIP4: Methodologies for Selection, Compilation and Analysis of Latest Paleocene and Early Eocene Climate Proxy Data, Incorporating Version 0.1 of the DeepMIP Database". In: *Geoscientific Model Development* 12.7, pp. 3149–3206. DOI: 10.5194/gmd-12-3149-2019 (cit. on p. 14).

Holmström, Max (2016). “Planktonic Foraminifera Biostratigraphy and Assemblage Analysis across the Eocene/Oligocene Boundary at IODP Site U1411, Newfoundland Margin”. MSc. Stockholm, Sweden: Stockholm University (cit. on p. 5).

Hu, Bin et al. (2014). “A Modified Procedure for Gas-Source Isotope Ratio Mass Spectrometry: The Long-Integration Dual-Inlet (LIDI) Methodology and Implications for Clumped Isotope Measurements”. In: *Rapid Communications in Mass Spectrometry* 28.13, pp. 1413–1425 (cit. on p. 10).

Huber, B.T. et al. (2016). “Pforams@microtax: A New Online Taxonomic Database for Planktonic Foraminifera”. In: *Micropaleontology* 62.6, pp. 429–438 (cit. on p. 6).

Huber, M. and R. Caballero (June 2011). “The Early Eocene Equable Climate Problem Revisited”. In: *Clim. Past* 7.2, pp. 603–633. DOI: 10.5194/cp-7-603-2011 (cit. on p. 22).

Hutchinson, David K. et al. (June 2018). “Climate Sensitivity and Meridional Overturning Circulation in the Late Eocene Using GFDL CM2.1”. In: *Climate of the Past* 14.6, pp. 789–810. DOI: 10.5194/cp-14-789-2018 (cit. on pp. 22, 25).

Hutchinson, David K. et al. (Aug. 2019). “Arctic Closure as a Trigger for Atlantic Overturning at the Eocene-Oligocene Transition”. In: *Nature Communications* 10.1, p. 3797. DOI: 10.1038/s41467-019-11828-z (cit. on pp. 3, 28).

Hutchinson, David K. et al. (Jan. 2021). “The Eocene–Oligocene Transition: A Review of Marine and Terrestrial Proxy Data, Models and Model–Data Comparisons”. In: *Clim. Past* 17.1, pp. 269–315. DOI: 10.5194/cp-17-269-2021 (cit. on pp. 3, 4, 6, 21, 25, 40).

Inglis, Gordon N. et al. (2015). “Descent toward the Icehouse: Eocene Sea Surface Cooling Inferred from GDGT Distributions”. In: *Paleoceanography* 30.7, pp. 1000–1020. DOI: 10.1002/2014PA002723 (cit. on p. 23).

Judd, Emily J., Tripti Bhattacharya, and Linda C. Ivany (2020). “A Dynamical Framework for Interpreting Ancient Sea Surface Temperatures”. In: *Geophysical Research Letters* n/a.n/a, e2020GL089044. DOI: 10.1029/2020GL089044 (cit. on p. 23).

Kim, Sang-Tae and James R. O’Neil (Aug. 1997). “Equilibrium and Nonequilibrium Oxygen Isotope Effects in Synthetic Carbonates”. In: *Geochimica et Cosmochimica Acta* 61.16, pp. 3461–3475. DOI: 10.1016/S0016-7037(97)00169-5 (cit. on pp. 14, 45).

Kobashi, Takuro et al. (Mar. 2004). "Water Mass Stability Reconstructions from Greenhouse (Eocene) to Icehouse (Oligocene) for the Northern Gulf Coast Continental Shelf (USA)". In: *Paleoceanography and Paleoclimatology* 19. DOI: 10.1029/2003PA000934 (cit. on pp. 4, 22).

Kocken, Ilja J. (Feb. 2019). *Clumped Isotope Data Analysis in R.* isoverse (cit. on p. 12).

Kocken, Ilja J., Inigo A. Müller, and Martin Ziegler (2019). "Optimizing the Use of Carbonate Standards to Minimize Uncertainties in Clumped Isotope Data". In: *Geochemistry, Geophysics, Geosystems* 20.11, pp. 5565–5577. DOI: 10.1029/2019GC008545 (cit. on p. 10).

Kopf, Sebastian (2020). *Isoreader: Read Stable Isotope Data Files.* isoverse (cit. on p. 12).

Kucera, Michal (Jan. 2007). "Chapter Six Planktonic Foraminifera as Tracers of Past Oceanic Environments". In: *Developments in Marine Geology.* Ed. by Claude Hillaire–Marcel and Anne De Vernal. Vol. 1. Proxies in Late Cenozoic Paleoceanography. Elsevier, pp. 213–262. DOI: 10.1016/S1572-5480(07)01011-1 (cit. on p. 8).

Lear, Caroline H. et al. (Mar. 2008). "Cooling and Ice Growth across the Eocene-Oligocene Transition". In: *Geology* 36.3, pp. 251–254. DOI: 10.1130/G24584A.1 (cit. on pp. 4, 22).

Leutert, Thomas J. et al. (July 2019). "Sensitivity of Clumped Isotope Temperatures in Fossil Benthic and Planktic Foraminifera to Diagenetic Alteration". In: *Geochimica et Cosmochimica Acta* 257, pp. 354–372. DOI: 10.1016/j.gca.2019.05.005 (cit. on pp. 4, 8, 11, 24, 41).

Liu, Zhonghui et al. (Feb. 2009). "Global Cooling During the Eocene-Oligocene Climate Transition". In: *Science* 323.5918, pp. 1187–1190. DOI: 10.1126/science.1166368 (cit. on pp. 4, 20, 21, 28).

Liu, Zhonghui et al. (Sept. 2018). "Transient Temperature Asymmetry between Hemispheres in the Palaeogene Atlantic Ocean". In: *Nature Geoscience* 11.9, p. 656. DOI: 10.1038/s41561-018-0182-9 (cit. on pp. 3, 20–24, 40).

Locarnini, Ricardo A. et al. (2019). *World Ocean Atlas 2018, Volume 1: Temperature.* Tech. rep. NOAA, 52p (cit. on pp. 5–7, 19, 22, 25, 26, 53).

Marchitto, T. M. et al. (Apr. 2014). "Improved Oxygen Isotope Temperature Calibrations for Cosmopolitan Benthic Foraminifera". In: *Geochimica et Cosmochimica Acta* 130, pp. 1–11. DOI: 10.1016/j.gca.2013.12.034 (cit. on p. 45).

Marzocchi, Alice et al. (Feb. 2015). “The North Atlantic Subpolar Circulation in an Eddy-Resolving Global Ocean Model”. In: *Journal of Marine Systems* 142, pp. 126–143. DOI: 10.1016/j.jmarsys.2014.10.007 (cit. on p. 14).

Meckler, A. Nele et al. (Aug. 2014). “Long-Term Performance of the Kiel Carbonate Device with a New Correction Scheme for Clumped Isotope Measurements: Performance and Correction of Kiel Clumped Isotope Measurements”. In: *Rapid Communications in Mass Spectrometry* 28.15, pp. 1705–1715. DOI: 10.1002/rcm.6949 (cit. on pp. 10, 12).

Meinicke, N. et al. (Feb. 2020). “A Robust Calibration of the Clumped Isotopes to Temperature Relationship for Foraminifers”. In: *Geochimica et Cosmochimica Acta* 270, pp. 160–183. DOI: 10.1016/j.gca.2019.11.022 (cit. on p. 13).

Meinicke, N. et al. (2021). “Coupled Mg/Ca and Clumped Isotope Measurements Indicate Lack of Substantial Mixed Layer Cooling in the Western Pacific Warm Pool During the Last ∼5 Million Years”. In: *Paleoceanography and Paleoclimatology* 36.8, e2020PA004115. DOI: 10.1029/2020PA004115 (cit. on pp. 13, 14, 17, 46).

Müller, Inigo A. et al. (June 2017a). “Carbonate Clumped Isotope Analyses with the Long-Integration Dual-Inlet (LIDI) Workflow: Scratching at the Lower Sample Weight Boundaries”. In: *Rapid Communications in Mass Spectrometry* 31.12, pp. 1057–1066. DOI: 10.1002/rcm.7878 (cit. on p. 10).

Müller, Inigo A. et al. (Jan. 2017b). “Clumped Isotope Fractionation during Phosphoric Acid Digestion of Carbonates at 70 °C”. In: *Chemical Geology* 449, pp. 1–14. DOI: 10.1016/j.chemgeo.2016.11.030 (cit. on p. 12).

Müller, R. Dietmar et al. (July 2018). “GPlates: Building a Virtual Earth Through Deep Time”. In: *Geochem. Geophys. Geosyst.* 19.7, pp. 2243–2261. DOI: 10.1029/2018GC007584 (cit. on p. 15).

Nooteboom, Peter D. et al. (2019). “Transport Bias by Ocean Currents in Sedimentary Microplankton Assemblages: Implications for Paleoceanographic Reconstructions”. In: *Paleoceanography and Paleoclimatology* 34.7, pp. 1178–1194. DOI: 10.1029/2019PA003606 (cit. on pp. 15, 26).

Nooteboom, Peter D. et al. (Sept. 2020). “Resolution Dependency of Sinking Lagrangian Particles in Ocean General Circulation Models”. In: *PLOS ONE* 15.9, e0238650. DOI: 10.1371/journal.pone.0238650 (cit. on p. 14).

Nooteboom, Peter Dirk et al. (Nov. 2021). *Strongly Eddying Ocean Simulations Required to Resolve Eocene Model-Data Mismatch*. Preprint. DOI: 10.1002/essoar.10508749.1 (cit. on pp. 14, 19, 26).

Norris, R.D. et al. (Mar. 2014). "Site U1411". In: *Proc. IODP*. Proceedings of the IODP 342. DOI: 10.2204/iodp.proc.342.112.2014 (cit. on pp. 4, 5, 41, 43).

Pearson, Paul N, Vlasta Premec-Fucek, and Isabella Premoli Silva (2006). "Taxonomy, Biostratigraphy, and Phylogeny of Eocene Turborotalia". In: *Atlas of Eocene planktonic foraminifera. Cushman Foundation Special Publication* 41, pp. 433–460 (cit. on p. 6).

Pearson, Paul N. et al. (Oct. 2001). "Warm Tropical Sea Surface Temperatures in the Late Cretaceous and Eocene Epochs". In: *Nature* 413.6855, pp. 481–487. DOI: 10.1038/35097000 (cit. on p. 8).

Pearson, Paul N. et al. (Mar. 2007). "Stable Warm Tropical Climate through the Eocene Epoch". In: *Geology* 35.3, pp. 211–214. DOI: 10.1130/G23175A.1 (cit. on p. 4).

Pearson, Paul N. et al. (Jan. 2018). "Taxonomy, Biostratigraphy, and Phylogeny of Oligocene Globanomalinidae (Pseudohastigerina and Turborotalia)". In: *Atlas of Oligocene Planktonic Foraminifera*. Cushman Foundation for Foraminiferal Research (cit. on p. 6).

Petersen, S. V. and D. P. Schrag (Oct. 2015). "Antarctic Ice Growth before and after the Eocene-Oligocene Transition: New Estimates from Clumped Isotope Paleothermometry". In: *Paleoceanography* 30.10, 2014PA002769. DOI: 10.1002/2014PA002769 (cit. on p. 4).

Piga, Emanuela (Feb. 2020). "How Hot Is Hot? Tropical Ocean Temperatures and Plankton Communities in the Eocene Epoch". PhD thesis. Cardiff University (cit. on pp. 4, 22).

Porta Mana, PierGianLuca and Laure Zanna (July 2014). "Toward a Stochastic Parameterization of Ocean Mesoscale Eddies". In: *Ocean Modelling* 79, pp. 1–20. DOI: 10.1016/j.ocemod.2014.04.002 (cit. on p. 14).

Prahl, Fredrick G, Laurel A Muehlhausen, and Debra L Zahnle (Sept. 1988). "Further Evaluation of Long-Chain Alkenones as Indicators of Paleoceanographic Conditions". In: *Geochimica et Cosmochimica Acta* 52.9, pp. 2303–2310. DOI: 10.1016/0016-7037(88)90132-9 (cit. on p. 23).

Project, Inkcape (2021). *Inkscape* (cit. on p. 9).

R Core Team (2020). *R: A Language and Environment for Statistical Computing.* R Foundation for Statistical Computing. Vienna, Austria (cit. on p. 12).

Rebotim, Andreia et al. (Feb. 2017). "Factors Controlling the Depth Habitat of Planktonic Foraminifera in the Subtropical Eastern North Atlantic". In: *Biogeosciences* 14.4, pp. 827–859. DOI: 10.5194/bg-14-827-2017 (cit. on pp. 8, 15).

Renaudie, Johan, David B. Lazarus, and Patrick Diver (Mar. 2020). "NSB (Neptune Sandbox Berlin): An Expanded and Improved Database of Marine Planktonic Microfossil Data and Deep-Sea Stratigraphy". In: *Palaeontol Electron* 23.1, pp. 1–28. DOI: 10.26879/1032 (cit. on pp. 5, 43).

Riveiros, Natalia Vázquez et al. (2016). "Mg/Ca Thermometry in Planktic Foraminifera: Improving Paleotemperature Estimations for G. Bulloides and N. Pachyderma Left". In: *Geochemistry, Geophysics, Geosystems* 17.4, pp. 1249–1264. DOI: 10.1002/2015GC006234 (cit. on p. 20).

Schmid, Thomas W. and Stefano M. Bernasconi (2010). "An Automated Method for 'Clumped-Isotope' Measurements on Small Carbonate Samples". In: *Rapid Communications in Mass Spectrometry* 24.14, pp. 1955–1963. DOI: 10.1002/rcm.4598 (cit. on p. 10).

Schmidt, Gavin .A., Grant R. Bigg, and Eelco J. Rohling (1999). *Global Seawater Oxygen-18 Database - v1.22* (cit. on p. 18).

Sexton, Philip F. and Paul A. Wilson (2009). "Preservation of Benthic Foraminifera and Reliability of Deep-Sea Temperature Records: Importance of Sedimentation Rates, Lithology, and the Need to Examine Test Wall Structure". In: *Paleoceanography* 24.2. DOI: 10.1029/2008PA001650 (cit. on p. 4).

Sexton, Philip F., Paul A. Wilson, and Paul N. Pearson (Dec. 2006). "Microstructural and Geochemical Perspectives on Planktic Foraminiferal Preservation: "Glassy" versus "Frosty"". In: *Geochem. Geophys. Geosyst.* 7.12, Q12P19. DOI: 10.1029/2006GC001291 (cit. on pp. 4, 24).

Shackleton, N J (1974). "Attainment of Isotopic Equilibrium between Ocean Water and the Benthic Foraminifera Genus Uvigerina: Isotopic Changes in the Ocean during the Last Glacial". In: *Colloques Internationaux du CNRS* 219, pp. 203–209 (cit. on p. 45).

Śliwińska, Kasia K. et al. (Dec. 2019). "Climate- and Gateway-Driven Cooling of Late Eocene to Earliest Oligocene Sea Surface Temperatures in the North Sea Basin".

In: *Sci Rep* 9.1, p. 4458. DOI: 10.1038/s41598-019-41013-7 (cit. on pp. 4, 20, 21).

Śliwińska, Kasia K. et al. (Jan. 2022). "Sea Surface Temperature Evolution of the North Atlantic Ocean across the Eocene-Oligocene Transition". In: *Climate of the Past Discussions*, pp. 1–24. DOI: 10.5194/cp-2021-184 (cit. on pp. 21, 22, 28).

Speijer, R. P. et al. (Jan. 2020). "Chapter 28 - The Paleogene Period". In: *Geologic Time Scale 2020*. Ed. by Felix M. Gradstein et al. Elsevier, pp. 1087–1140. DOI: 10.1016/B978-0-12-824360-2.00028-0 (cit. on pp. 16, 43).

Takahashi, Kozo and Allan W.H. Be (Dec. 1984). "Planktonic Foraminifera: Factors Controlling Sinking Speeds". In: *Deep Sea Research Part A. Oceanographic Research Papers* 31.12, pp. 1477–1500. DOI: 10.1016/0198-0149(84)90083-9 (cit. on p. 15).

Tierney, Jessica E. and Martin P. Tingley (2018). "BAYSPLINE: A New Calibration for the Alkenone Paleothermometer". In: *Paleoceanography and Paleoclimatology* 33.3, pp. 281–301. DOI: 10.1002/2017PA003201 (cit. on p. 23).

Tierney, Jessica E. et al. (Aug. 2017). "Eocene Temperature Gradients". In: *Nature Geoscience* 10.8, pp. 538–539. DOI: 10.1038/ngeo2997 (cit. on p. 23).

Tierney, Jessica E. et al. (Aug. 2020a). "Glacial Cooling and Climate Sensitivity Revisited". In: *Nature* 584.7822, pp. 569–573. DOI: 10.1038/s41586-020-2617-x (cit. on pp. 20, 21).

Tierney, Jessica E. et al. (Nov. 2020b). "Past Climates Inform Our Future". In: *Science* 370.6517. DOI: 10.1126/science.aay3701 (cit. on p. 23).

Tolderlund, Douglas S. and Allan W. H. Bé (1971). "Seasonal Distribution of Planktonic Foraminifera in the Western North Atlantic". In: *Micropaleontology* 17.3, pp. 297–329. DOI: 10.2307/1485143 (cit. on p. 8).

Torsvik, Trond H. et al. (Sept. 2012). "Phanerozoic Polar Wander, Palaeogeography and Dynamics". In: *Earth-Science Reviews* 114.3, pp. 325–368. DOI: 10.1016/j.earscirev.2012.06.007 (cit. on p. 15).

van der Weijst, Carolien M. H. et al. (Sept. 2021). "A Fifteen-Million-Year Surface- and Subsurface-Integrated TEX_{86} Temperature Record from the Eastern Equatorial Atlantic". In: *Climate of the Past Discussions*, pp. 1–23. DOI: 10.5194/cp-2021-92 (cit. on p. 23).

van Sebille, Erik et al. (Mar. 2015). "Ocean Currents Generate Large Footprints in Marine Palaeoclimate Proxies". In: *Nature Communications* 6.1, p. 6521. DOI: 10.1038/ncomms7521 (cit. on pp. 14, 15).

Wade, Bridget S. and Paul N. Pearson (Aug. 2008). "Planktonic Foraminiferal Turnover, Diversity Fluctuations and Geochemical Signals across the Eocene/Oligocene Boundary in Tanzania". In: *Marine Micropaleontology* 68.3, pp. 244–255. DOI: 10.1016/j.marmicro.2008.04.002 (cit. on p. 5).

Wade, Bridget S. et al. (Feb. 2012). "Multiproxy Record of Abrupt Sea-Surface Cooling across the Eocene-Oligocene Transition in the Gulf of Mexico". In: *Geology* 40.2, pp. 159–162. DOI: 10.1130/G32577.1 (cit. on pp. 4, 22).

Wade, Bridget S. et al. (2018). "Taxonomy, Biostratigraphy, and Phylogen of Oligocene and Lower Miocene Dentoglobigerina and Globoquadrina". In: *Atlas of Oligocene Planktonic Foraminifera*. Vol. 46. Cushman Foundation of Foraminiferal Research, pp. 331–384 (cit. on pp. 5, 6).

Westerhold, Thomas et al. (Sept. 2020). "An Astronomically Dated Record of Earth's Climate and Its Predictability over the Last 66 Million Years". In: *Science* 369.6509, pp. 1383–1387. DOI: 10.1126/science.aba6853 (cit. on pp. 3, 15–17, 21).

WOCE Hydrographic Programme, W. H. P. (Oct. 2002). *Hydrochemistry Measured on Water Bottle Samples during HUDSON Cruise 18HU95003_1 on Section AR13*. DOI: 10.1594/PANGAEA.837450 (cit. on p. 53).

Zachos, James et al. (Apr. 2001). "Trends, Rhythms, and Aberrations in Global Climate 65 Ma to Present". In: *Science* 292.5517, pp. 686–693. DOI: 10.1126/science.1059412 (cit. on p. 3).

Zachos, James C., Gerald R. Dickens, and Richard E. Zeebe (Jan. 2008). "An Early Cenozoic Perspective on Greenhouse Warming and Carbon-Cycle Dynamics". In: *Nature* 451.7176, pp. 279–283. DOI: 10.1038/nature06588 (cit. on p. 3).

Zhang, Yi Ge and Xiaoqing Liu (2018). "Export Depth of the TEX86 Signal". In: *Paleoceanography and Paleoclimatology* 33.7, pp. 666–671. DOI: 10.1029/2018PA003337 (cit. on p. 23).

8 Supporting information for "North Atlantic temperature change across the Eocene–Oligocene Transition"

Contents of this file

- Section S8.1
- Figure S1 to Figure S16
- Table S1

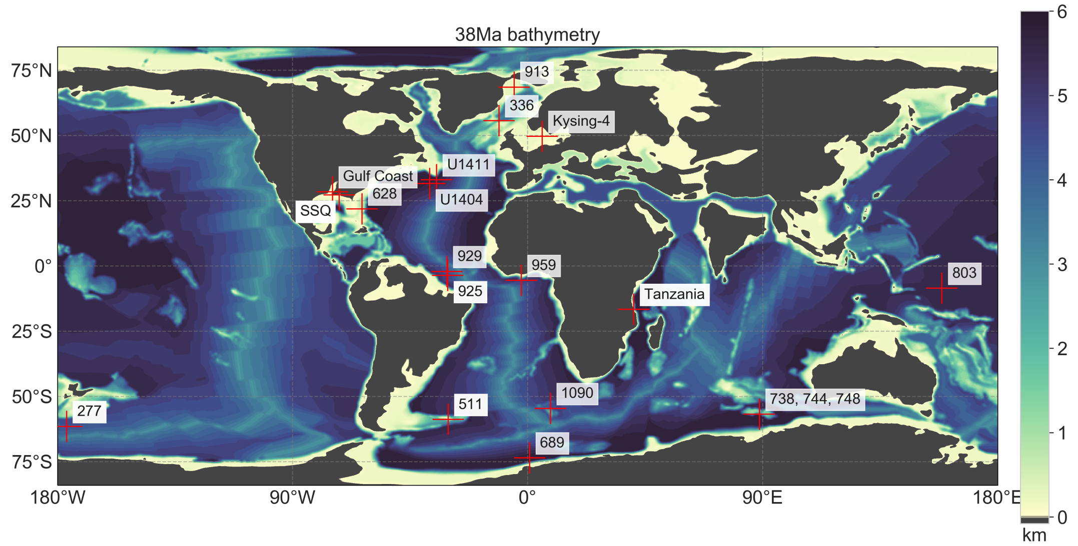

Figure S1. Paleobathymetry of Baatsen et al. (2016) for 38 Ma, with reconstructed drill site locations from the latitudinal composite of Hutchinson et al. (2021).

S8.1 Foraminifera preservation mass-balance calculation

If the foraminifera would have been affected by deep-sea dissolution and recrystallisation, we can estimate how much of the test material would have to be overprinted by a simple mass-balance calculation for the worst-case scenario: assuming deep-sea temperatures (DST) of 0.0 °C (the modern ocean values at this site, so likely warmer during the Eocene) and SST estimates of 28 °C (Liu et al., 2018).

$$\mathrm{SST_{rec}} = (1-\alpha)\mathrm{SST} + \alpha\mathrm{DST}, \tag{2}$$

Table S1. Average stable isotope results for the mixed-layer (M) dwelling foraminifera and the thermocline (T) dwelling foraminifera across the EOT.

	Age (Ma)	N	$\delta^{13}C$ (VPDB)	$\delta^{18}O$ (VPDB)	Δ_{47} (‰ I-CDES)	T (°C)	$\delta^{18}O_{sw}$ (VSMOW)
M	32.5	22	0.76 ± 0.081	0.39 ± 0.26	0.63 ± 0.017	13 ± 5.2	0.32 ± 1.4
M	33.6	72	1.5 ± 0.039	0.42 ± 0.06	0.62 ± 0.0073	17 ± 2.3	1.1 ± 0.55
M	33.7	52	0.85 ± 0.046	-0.19 ± 0.071	0.61 ± 0.012	18 ± 3.8	0.79 ± 0.87
M	35.1	43	0.67 ± 0.051	-0.33 ± 0.076	0.61 ± 0.012	18 ± 4	0.61 ± 0.91
T	32.5	28	0.79 ± 0.055	1.3 ± 0.18	0.63 ± 0.016	14 ± 5	1.4 ± 1.3
T	33.6	37	1.3 ± 0.035	1.4 ± 0.1	0.64 ± 0.014	10 ± 4.1	0.6 ± 1
T	33.7	31	0.75 ± 0.034	0.17 ± 0.071	0.63 ± 0.016	14 ± 5	0.32 ± 1.2
T	35.1	24	0.64 ± 0.04	-0.17 ± 0.089	0.61 ± 0.013	20 ± 4.3	1.2 ± 0.98

where SST_{rec} is the reconstructed SST, and thus:

$$\alpha = (SST_{rec} - SST)/(DST - SST). \tag{3}$$

To arrive at our reconstructed Eocene SST of 18 °C, an overprinting of more than 42 % would be required. Figure S2 shows the overprinting factor required under different assumptions for the deep sea temperature (−1.9 °C, the minimum sea water temperature prior to freezing up to 8 °C) and the assumed true SST. Most of these scenarios require at least 10 % overprinting to achieve the clumped-isotope derived temperatures we arrive at. Given the photographic evidence and the previous studies of the excellent preservation at this site (Leutert et al., 2019; Norris et al., 2014), this is highly unlikely.

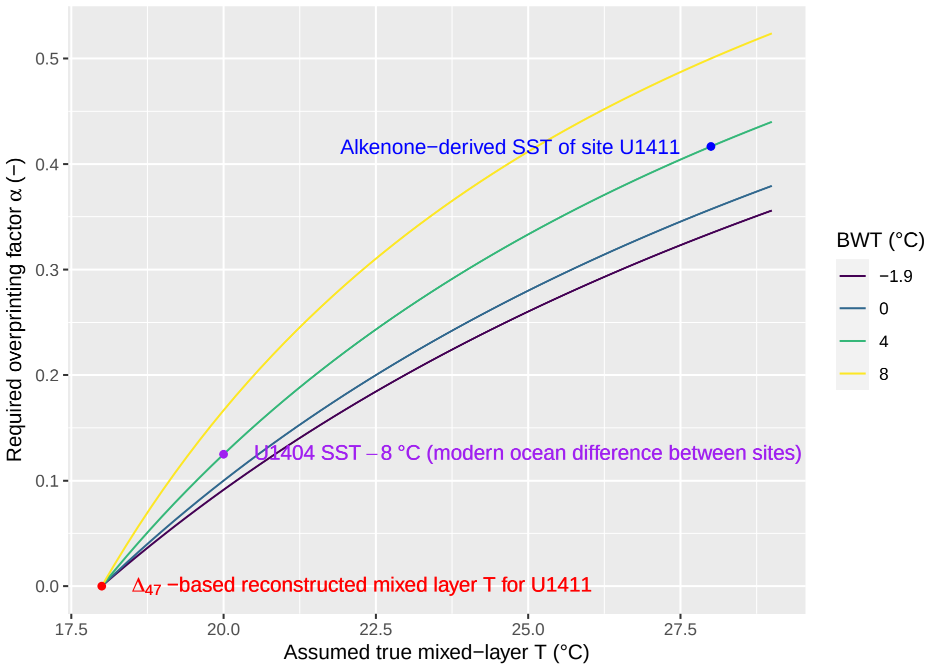

Figure S2. Overprinting factor α required to arrive at final clumped-isotope based temperature under different 'true' sea surface temperature assumptions (x-axis) and bottom water temperature assumptions (colour).

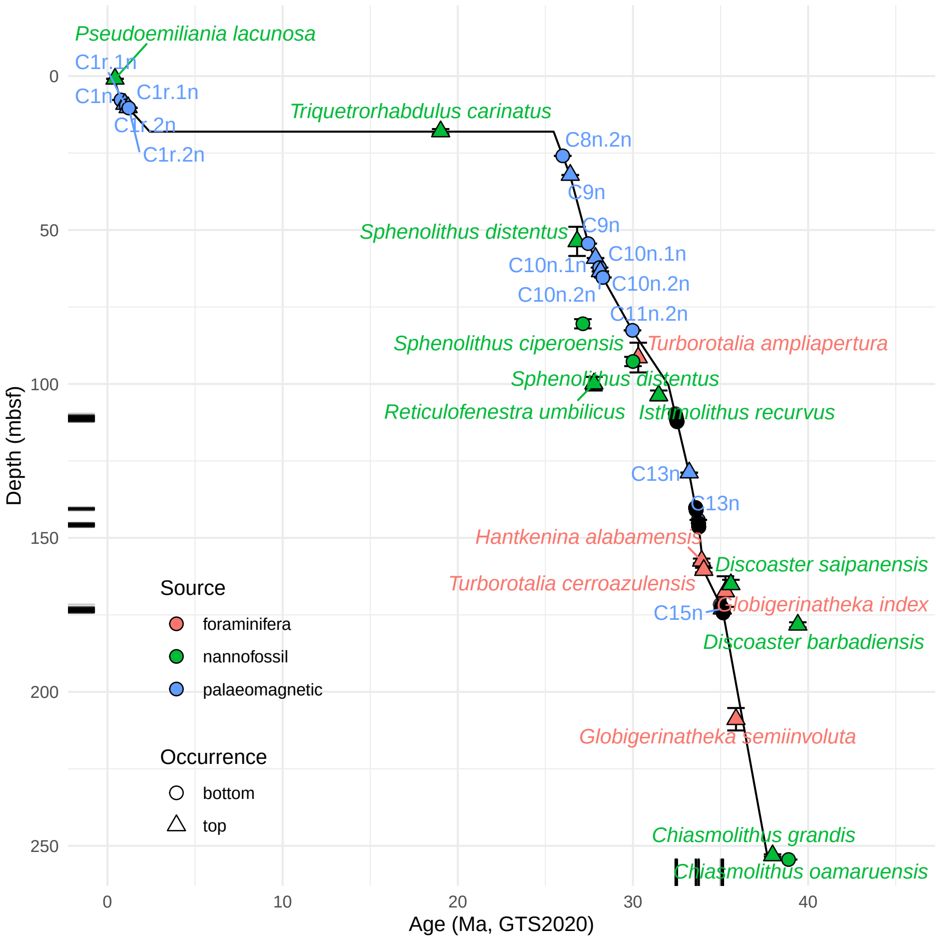

Figure S3. The age model for IODP site U1411 is based on the shipboard age model (Norris et al., 2014) with adjustments from the Neptune database (Renaudie, Lazarus, & Diver, 2020) presented on the Geological Time Scale 2020 (Speijer et al., 2020). The black line represents the age model, with the tops (triangles) and bottoms (circles) of foraminifera (red), nannofossil (green), and magnetic polarity chrons (blue). Black points and segments near the axes represent the samples analyzed in this study.

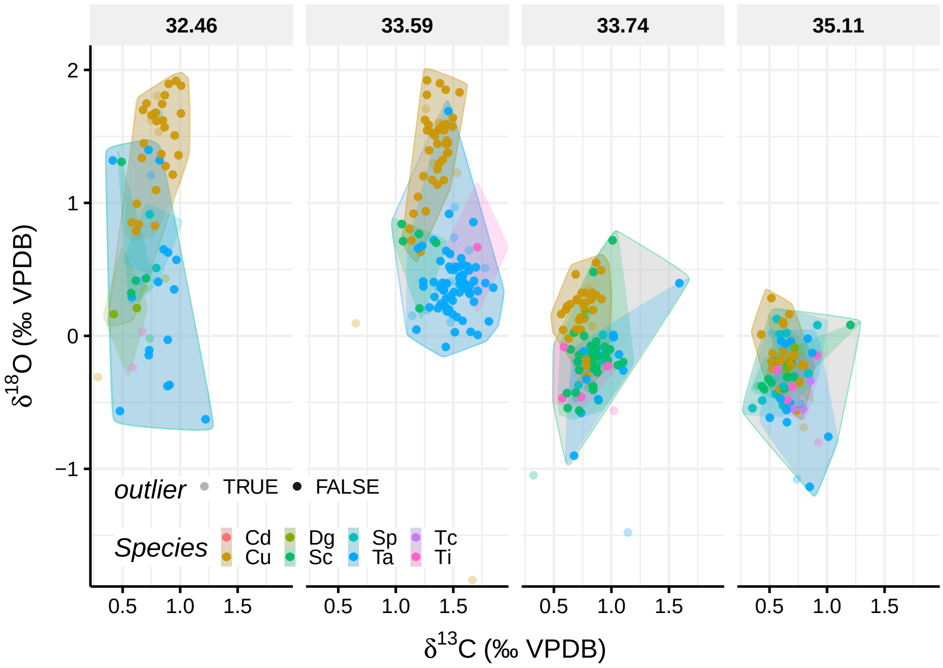

Figure S4. The planktic foraminifera of IODP site U1411 that group together on the δ^{13}C and δ^{18}O scales were averaged for clumped isotope analysis. Columns indicate the average sample time-period in Ma. Cd = *C. dissimilis*, Cu = *C. unicavus*, Dg = *D. galivasi*, Sc = *S. corpulenta*, Sp = *S. projecta*, Ta = *T. ampliapertura*, Tc = , Ti = *T. increbescens*.

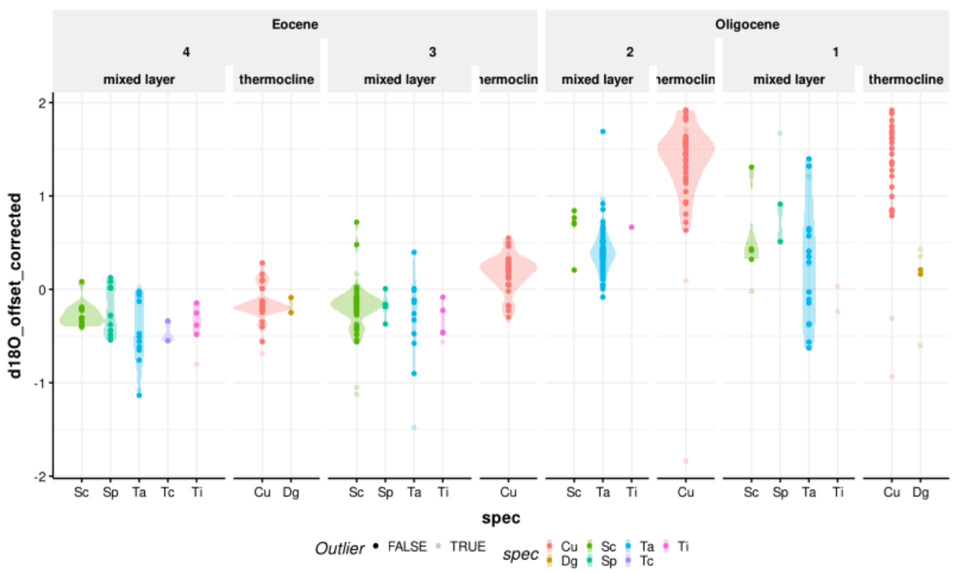

Figure S5. Species assignment based on δ^{18}O values across the 4 sampled intervals. Note that we changed the assigned dwelling depths of *S. corpulenta* and *S. projecta* because they appeared to agree better with *T. ampliapertura* values than with *C. unicavus* (Figure S5).

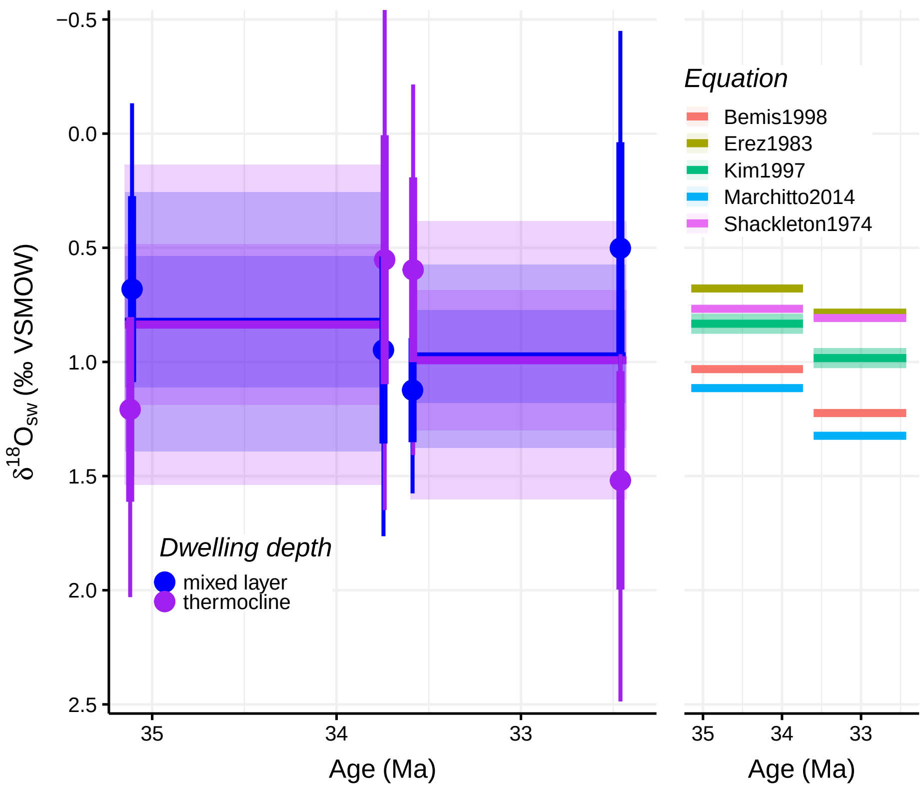

Figure S6. $\delta^{18}O_{sw}$ estimates inherit their large uncertainty from the Δ_{47} temperatures. The right hand panel shows the effect of choosing a different equation that relates $\delta^{18}O_{cc}$ and temperature to $\delta^{18}O_{sw}$ (Bemis et al., 1998; Erez & Luz, 1983; Kim & O'Neil, 1997; Marchitto et al., 2014; Shackleton, 1974). Our preferred equation is highlighted in green.

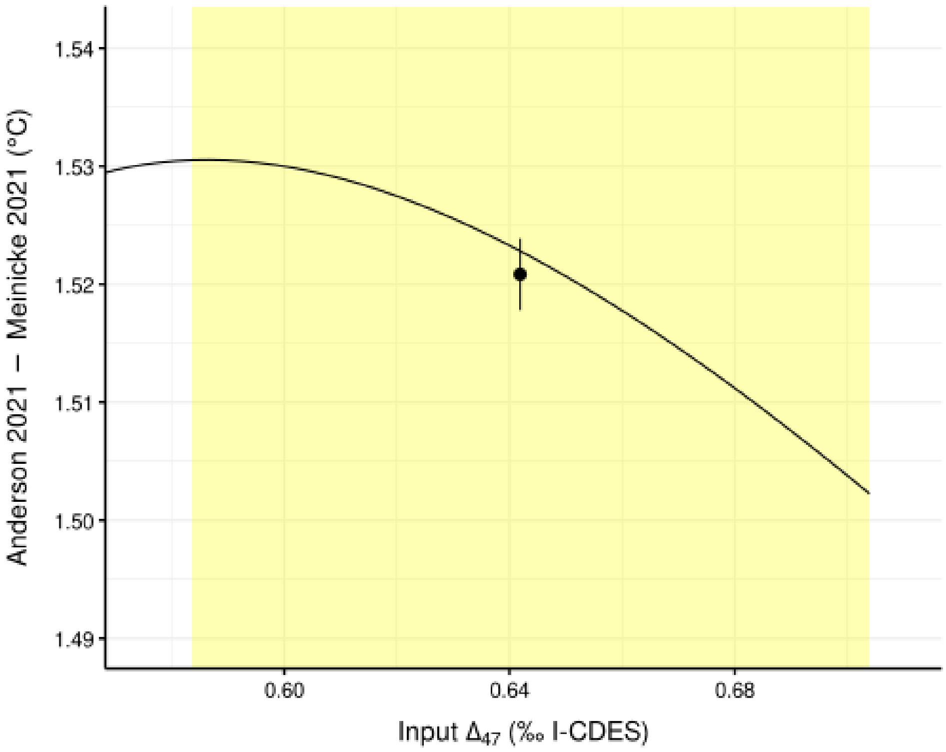

Figure S7. Comparison between the Anderson et al. (2021) and Meinicke et al. (2021) calibrations for the temperature range of interest for palaeoclimate reconstructions (yellow rectangle).

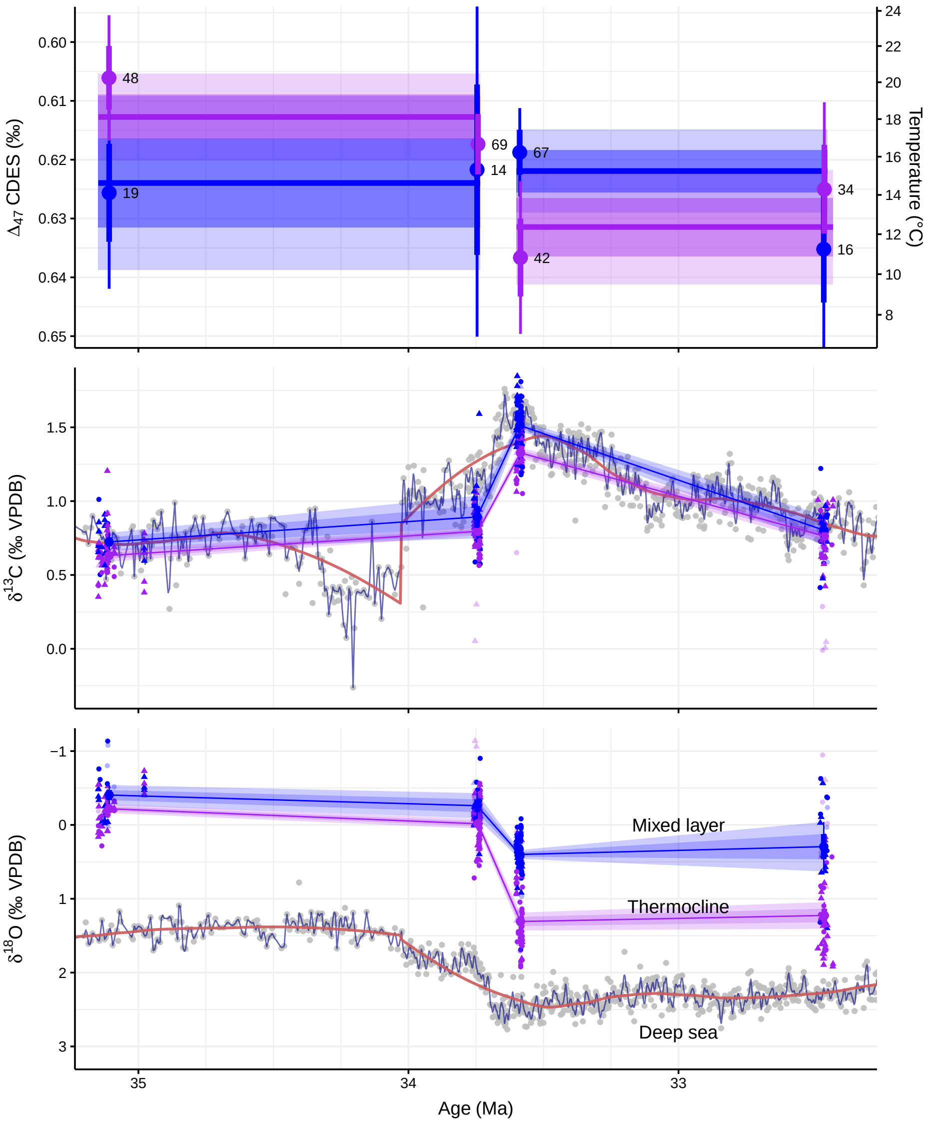

Figure S8. Same as Figure 4, but calculated based on previous depth associations of the different foraminifera species from Table 1.

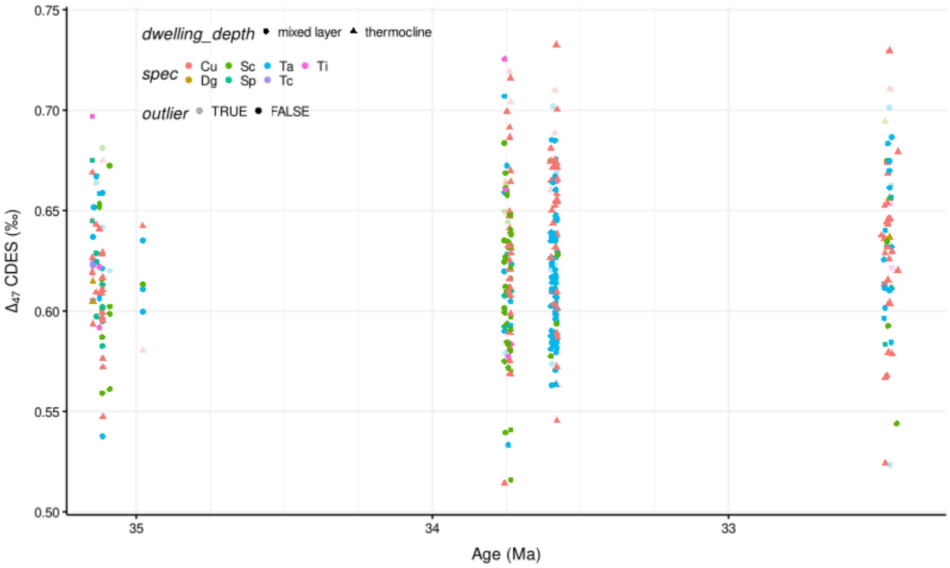

Figure S9. All replicate clumped isotope points used to generate averages.

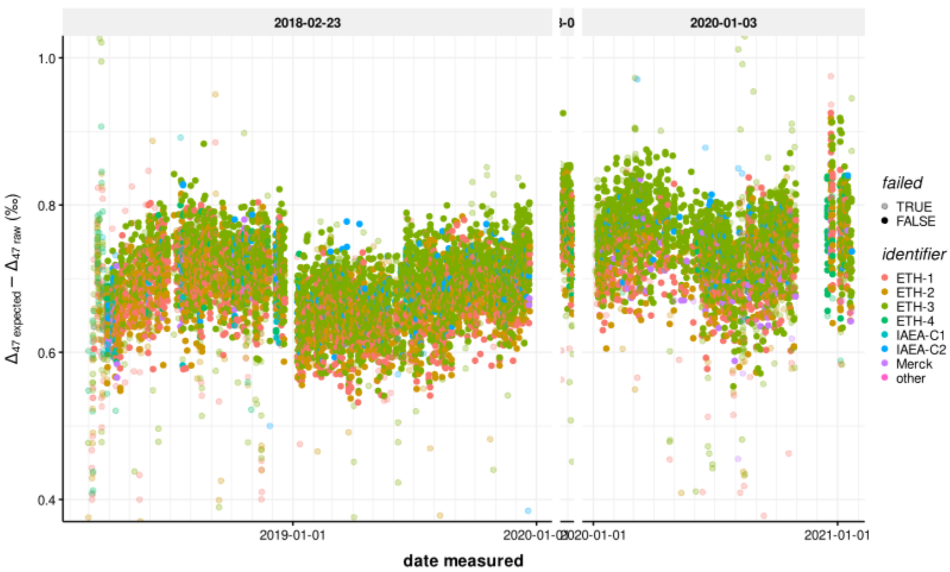

Figure S10. Offset correction criteria for the whole measuement range.

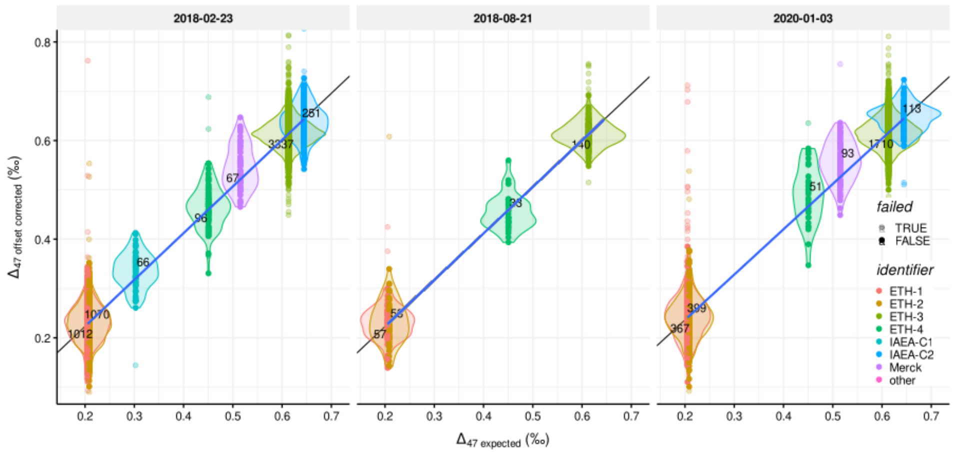

Figure S11. Empirical transfer functions for the sessions at UU (left and right) and at UiB (middle).

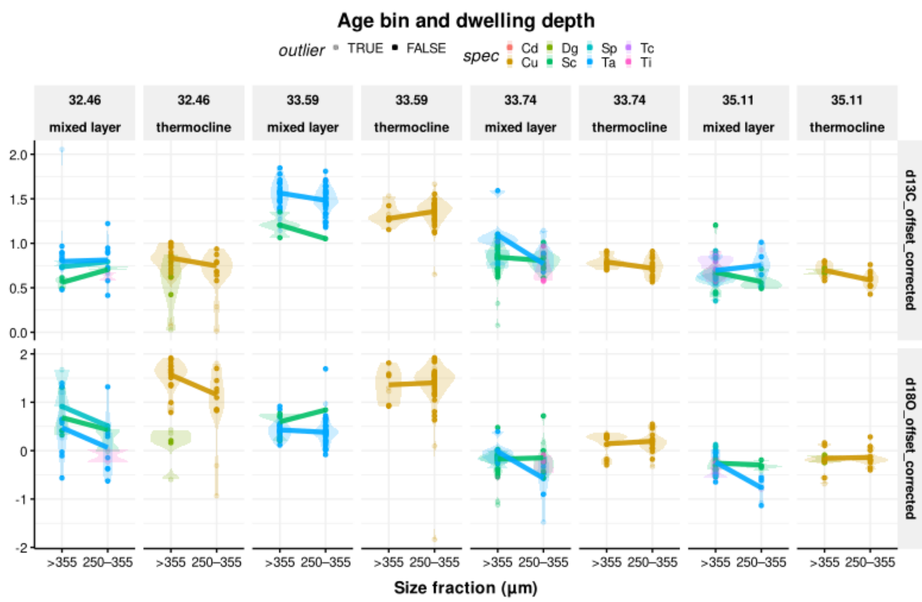

Figure S12. Size fractions were binned for clumped isotope analysis because there was no systematic offset.

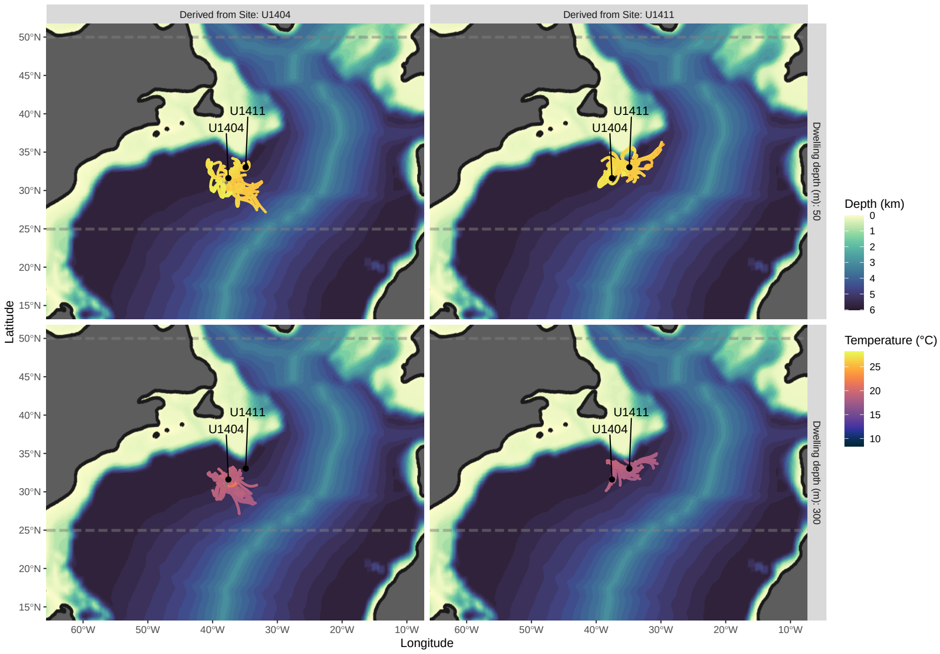

Figure S13. Advective transport for the simulated particles released near the paleolocation of IODP site U1411, with foraminifera dwelling depths of 50 and 300 m (panels). Colour indicates the temperature that the particle is exposed to at that point in time. Also shown is the bathymetry.

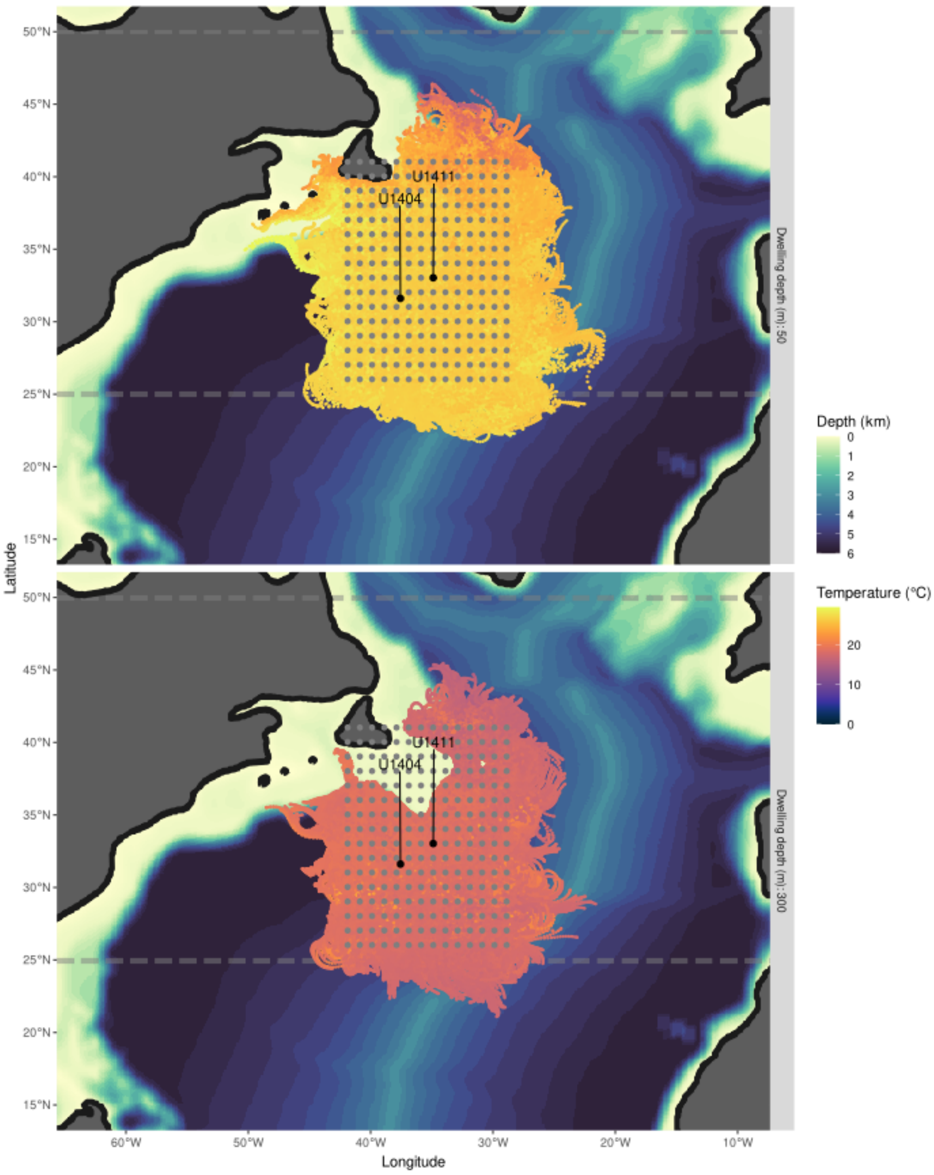

Figure S14. Same as Figure S13 but showing the whole grid of simulated points.

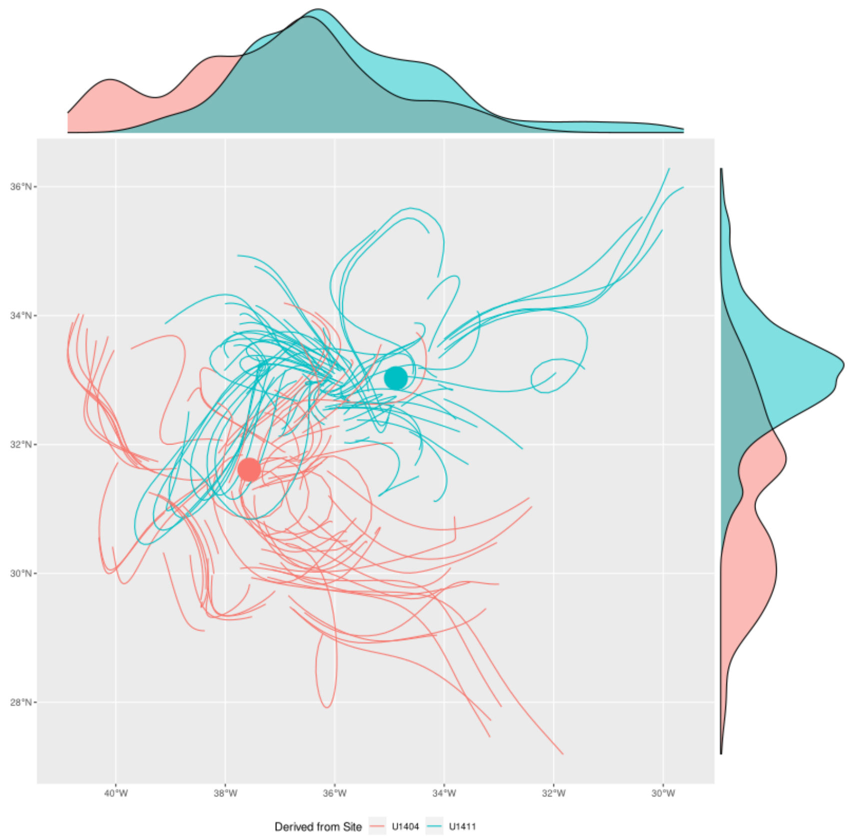

Figure S15. Particles that ultimately arrive at site U1411 show an overlap with those that arrive near site U1404 in longitude and latitude.

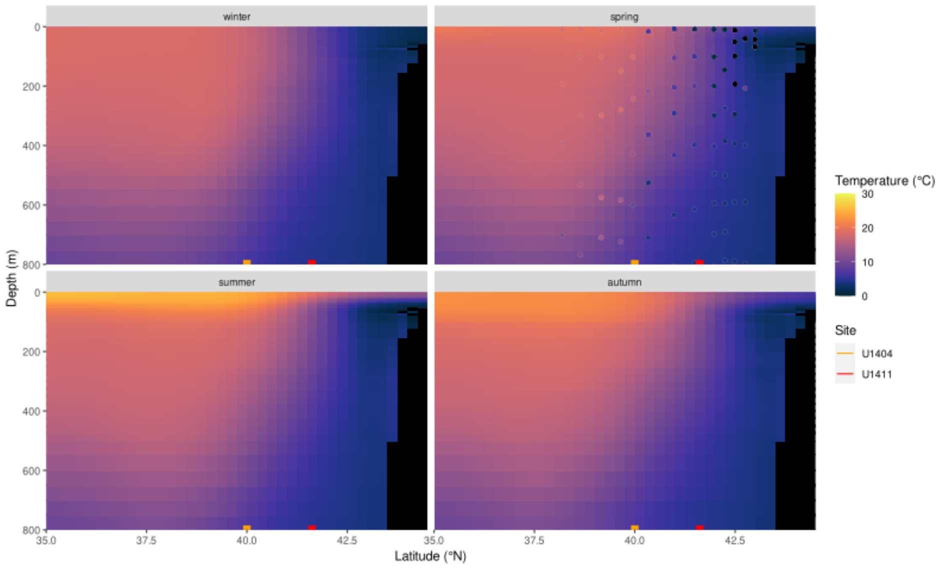

Figure S16. Modern ocean temperature profile of the North Atlantic along the longitude near that of site U1411 (red rectangle) (Locarnini et al., 2019) and site 1404 (orange rectangle) with CTD data (coloured points) from April and May of 1995 between 50.9°E and 49.8°E from WOCE Hydrographic Programme, 2002.